Patterns of Precipitation and Mesolow Evolution in Midlatitude Mesoscale Convective Vortices

ERIC P. JAMES AND RICHARD H. JOHNSON

Department of Atmospheric Science, Colorado State University, Fort Collins, Colorado

(Manuscript received 29 May 2009, in final form 23 September 2009)

ABSTRACT

Surface pressure manifestations of mesoscale convective vortices (MCVs) that traversed Oklahoma during the periods May–August 2002–05 are studied using the Weather Surveillance Radar-1988 Doppler (WSR-88D), the Oklahoma Mesonet, and the NOAA Profiler Network data. Forty-five MCVs that developed from mesoscale convective systems (MCSs) have been investigated, 28 (62%) of which exhibit mesolows detectable at the surface. Within this group, three distinct patterns of precipitation organization and associated mesolow evolution have been identified. The remaining 17 (38%) of the cases do not contain a surface mesolow. Two repeating patterns of precipitation organization are identified for the latter group.

The three categories of MCVs possessing a surface mesolow are as follows. Nineteen are classified as ''rear-inflow-jet MCVs,'' and tend to form within large and intense asymmetric MCSs. Rear inflow into the MCS, enhanced by the development of an MCV on the left-hand side relative to system motion, produces a rear-inflow notch and a distinct surface wake low at the back edge of the stratiform region. Hence, the surface mesolow and MCV are displaced from one another. Eight are classified as ''collapsing-stratiform-region MCVs.'' These MCVs arise from small asymmetric MCSs. As the stratiform region of the MCS weakens, a large mesolow appears beneath its dissipating remnants due to broad subsidence warming, and at the same time the midlevel vortex spins up due to column stretching. One case, called a ''vertically coherent MCV,'' contains a well-defined surface mesolow and associated cyclonic circulation, apparently due to the strength of the midlevel warm core and the weakness of the low-level cold pool. In these latter two cases, the surface mesolow and MCV are approximately collocated.

Within the group of MCVs without a surface mesolow, 14 are classified as ''remnant-circulation MCVs'' containing no significant precipitation or surface pressure effects. Finally, three are classified as ''cold-pool-dominated MCVs;'' these cases contain significant precipitation but no discernible surface mesolow.

This study represents the first systematic analysis of the surface mesolows associated with MCVs. The pattern of surface pressure and winds accompanying MCVs can affect subsequent convective development in such systems. Extension of the findings herein to tropical oceans may have implications regarding tropical cyclogenesis.

1. Introduction

Mesoscale convective vortices (MCVs) are a commonly observed and well-documented feature of mature to decaying mesoscale convective systems (MCSs) in both the midlatitudes (e.g., Johnston 1982) and the tropics (e.g., Houze and Betts 1981). In terms of potential vorticity (PV) thinking, MCVs are the balanced response to the increasing latent heating with height in the stratiform regions of MCSs (Hertenstein and Schubert 1991). Many MCV formation mechanisms have been proposed in the literature based on terms in the vorticity equation. Additionally, the reduction of the Rossby radius of deformation due to the low static stability in the moist stratiform regions of MCSs may be necessary for MCV formation (Chen and Frank 1993). Recent studies have demonstrated that MCVs follow a variety of developmental paths (Kirk 2003, 2007), which suggests that multiple distinct MCV types may exist.

The successful detection and prediction of MCVs is important from an operational forecasting perspective because of their influence on the potential for, and organization of, deep, moist convection (e.g., Schumacher and Johnson 2008). The midlevel PV anomaly associated with an MCV can interact with vertical wind shear

Corresponding author address: Eric James, Department of Atmospheric Science, Colorado State University, 1371 Campus Delivery, Fort Collins, CO 80523-1371.
E-mail: ejames@atmos.colostate.edu

DOI: 10.1175/2009MWR3076.1

in such a way that the resulting balanced lifting locally favors the regeneration of convection downshear of the vortex (Raymond and Jiang 1990), thereby intensifying latent heat release and strengthening the MCV (e.g., Fritsch et al. 1994; Trier and Davis 2002; Davis and Trier 2002). MCVs have also been found to play a role in the organization of convection in quasi-stationary, backbuilding MCSs that produce extreme rainfall (Schumacher and Johnson 2008, 2009).

There have been abundant studies examining the surface features of MCSs over the past 80 years (Johnson 2001), but only a few investigating the particular surface features that accompany MCVs. Most of these have been based on data from the Oklahoma–Kansas Preliminary Regional Experiment for Storm-Scale Operational and Research Meteorology (OK PRE-STORM; Cunning 1986) during the summer of 1985, which provided the first high-resolution surface observations of MCSs and their associated MCVs.

An investigation of the 23–24 June 1985 OK PRE-STORM MCS by Johnson et al. (1989) found several interesting surface features associated with the decay of the MCS and the development of a midlevel circulation. There was a strong mesohigh situated beneath the stratiform region of the MCS during its mature phase. As the stratiform rain degenerated, this mesohigh rapidly transformed into a strong mesolow (see Johnson et al. 1989, their Fig. 12). This transformation was coincident with the appearance of a well-defined cyclonic vortex in visible satellite imagery. The authors proposed that the mesolow was the hydrostatic response to warming within a region of strong mesoscale subsidence in the absence of precipitation; this warm subsiding air produced localized ''heat bursts'' at several mesonet stations (Bernstein and Johnson 1994). The existence of unsaturated downdrafts driven by rainfall evaporation has been demonstrated in a well-known modeling study (Brown 1979), and is understood to be the mechanism for both microbursts (McNulty 1991) and heat bursts (Johnson 1983).

Brandes (1990) and Brandes and Ziegler (1993) studied the 6–7 May 1985 OK PRE-STORM MCS. They found that the associated MCV focused and intensified a descending rear-inflow jet (RIJ) into the southern portion of the system. This subsiding air current led to strong low-level warming and drying, producing a mesolow with a perturbation pressure anomaly of −4 hPa (see Brandes 1990, his Fig. 18). They also found that the MCV was amplified by convergence into the mesoscale downdraft associated with the MCS. The mesolow within this system was a ''wake low,'' of the type studied by Johnson and Hamilton (1988). These lows result hydrostatically from concentrated descent within a RIJ; evaporational cooling at the rear of the stratiform region induces subsidence in the jet, which eventually becomes unsaturated and warms adiabatically (Stumpf et al. 1991).

TABLE 1. Mean values of structural characteristics of the five independent MCV types defined in this paper. Longevity is defined as the number of hours the MCV is detected by the objective algorithm. Vortex radius (see DAT for definition) and relative vorticity (mean over the 600–500-hPa layer) are determined for each case at the time when the MCV reaches its maximum relative vorticity at any level between 600 and 500 hPa. Statistical significance (indicated with superscripts) is assessed by means of a one-tailed Student's *t* test.

MCV type	No.	Percentage	Longevity (h)	Radius (km)	Relative vorticity (s^{-1})
All MCVs	45	100	17	225	9.98×10^{-5}
RIJ[a]	19	42	15	231	1.32×10^{-4}[g]
CSR[b]	8	18	14	206[h]	6.75×10^{-5}[h]
VC[c]	1	2	10	262	8.83×10^{-5}
RC[d]	14	31	24[f]	225	8.21×10^{-5}
CPD[e]	3	7	13	227	7.92×10^{-5}

[a] Rear-inflow-jet MCV.
[b] Collapsing-stratiform-region MCV.
[c] Vertically coherent MCV.
[d] Remnant-circulation MCV.
[e] Cold-pool-dominated MCV.
[f] Significantly different from the mean of all the MCVs at the 90% level.
[g] Significantly different from the mean of all the MCVs at the 99% level.
[h] Significantly different from the mean of all the MCVs at the 95% level.

Recently, Galarneau et al. (2009) have demonstrated that MCVs can undergo ''baroclinic transition'' in which they acquire surface fronts due to upper-level forcing. This process leads to surface low development by baroclinic mechanisms, and has also been documented by Zhang and Harvey (1995).

While many studies have described the structure and evolution of individual MCV cases, there has not been any attempt to classify MCVs into recurring types. The success of classification schemes concerning MCS evolution suggests that this may be a useful avenue of MCV research. Houze et al. (1990) introduced terminology classifying MCSs based on their adherence to the frequently observed ''leading-line/trailing-stratiform'' precipitation structure. They also noted the existence of asymmetric systems, in which the stratiform rainfall is predominantly on the poleward side of the MCS; this asymmetry may reflect the presence of an embedded mesovortex (see Houze et al. 1989, their Fig. 2b). Parker and Johnson (2000) classified central U.S. MCSs into three modes based on the position of the stratiform region with respect to system motion. These classification schemes have provided a basis for further investigation

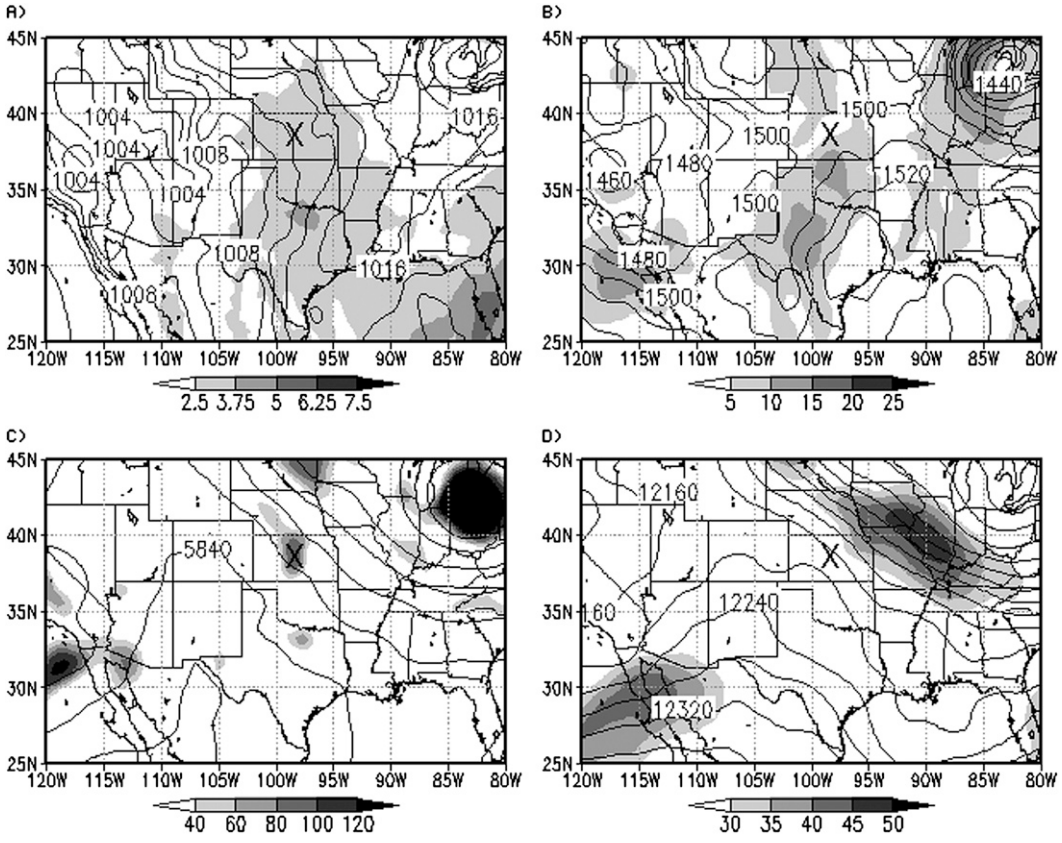

FIG. 1. RUC analysis of (a) mean sea level pressure (hPa; contour interval 2 hPa) and column-integrated precipitable water (cm; shaded, with scale at bottom), (b) 850-hPa geopotential height (m; contour interval 10 m) and isotachs (m s^{-1}; shaded, with scale at bottom), (c) 500-hPa geopotential height (m; contour interval 40 m) and relative vorticity (10^{-6} s^{-1}; shaded, with scale at bottom), and (d) 200-hPa geopotential height (m; contour interval 40 m) and isotachs (m s^{-1}; shaded, with scale at bottom) at 1200 UTC 24 May 2003. Location of developing MCV is marked by a large cross in (a)–(d).

into MCS organization, and have been adopted by the operational community. The variety of MCV structures and evolutions reported in the literature supports the possibility of a meaningful classification scheme for these systems.

This work presents several MCV archetypes and their associated surface pressure characteristics, based on dense surface and upper-air observations of midlatitude MCVs. We believe that such a classification scheme will be useful to the operational community for forecasting purposes, as well as serve as a basis for further investigations of MCV dynamics. While mesohighs exist in the vicinity of MCVs, our focus is on the formation and evolution of mesolows because of their potential dynamical linkage with the overlying MCV. The remainder of this paper is organized as follows. Section 2 describes the methodology followed for selecting, analyzing, and classifying the individual MCV cases. Results are presented in section 3, and discussed in section 4. Section 5 contains some conclusions.

2. Methodology

To enable a useful classification of MCVs, it is important to find a large number of cases to examine in detail. An automated MCV detection algorithm, developed by Davis et al. (2002, hereafter DAT), is used to identify cases. This algorithm operates on analyses from the Rapid Update Cycle (RUC) model (Benjamin et al. 2004); details are provided in DAT. The original algorithm operates on the relative vorticity field averaged over the three model levels of 600, 550, and 500 hPa; for this study, the presence of numerous missing levels in the RUC data prompted a modification of the algorithm to search for MCVs based on only one or two of the three model levels if necessary. The algorithm is run on hourly RUC analyses (with 40-km horizontal resolution) during the months of May–August of the years 2002–05. At each time, the algorithm produces a map of relative vorticity maxima that satisfy certain structural criteria (including exceeding a ''roundness'' threshold and falling below a

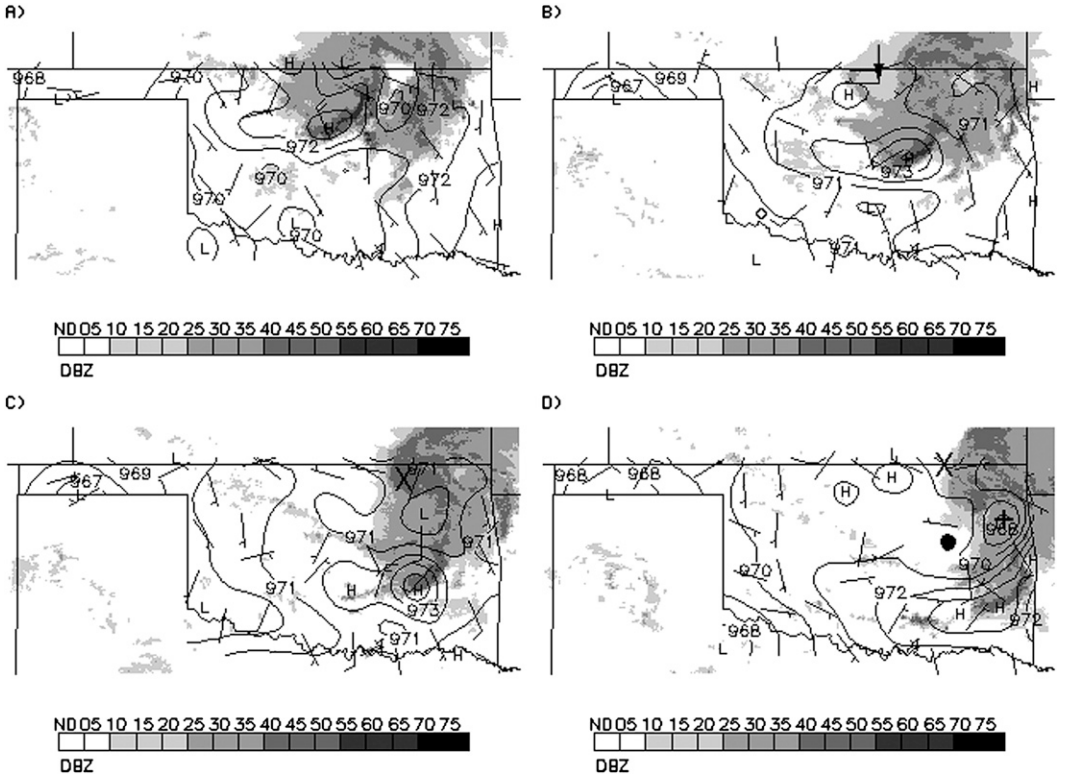

FIG. 2. OM surface pressure analyses (hPa; contour interval 1 hPa) overlaid on OM observed 10-m wind barbs (short barb 2.5 m s^{-1}; long barb 5 m s^{-1}) and WSR-88D composite radar reflectivity (dB*Z*; shaded, with scale at bottom) at (a) 1400, (b) 1500, (c) 1600, and (d) 1700 UTC 24 May 2003. Pressure is adjusted to 356.6-m elevation. The midlevel MCV center, as detected by RUC algorithm, is marked by a large cross in (c),(d). In (b), black arrow indicates location of developing rear inflow notch. The Tahlequah OM station is marked by a plus sign in (d). The Haskell NPN station is marked by a filled circle in (d). ''H'' and ''L'' indicate centers of high and low pressure, respectively.

mesoscale size threshold); these vortices can be tracked between analysis times. For each detected vortex, radar and satellite imagery are examined to determine if the vortex is in fact an MCV. Detected vortices are considered MCVs if they are embedded within, or arise from, significant stratiform precipitation and anvil cloud associated with deep, moist convection. This definition is inevitably subjective, but all of the vortices detected by the algorithm are clearly MCVs or clearly not. We search for MCVs within a latitude–longitude box containing the state of Oklahoma. Climatological characteristics of the detected MCVs will be reported in a forthcoming paper.

Once a list of MCV cases has been compiled, a detailed analysis of each case is carried out based on data from the Oklahoma Mesonet (OM; 5-minute observations) and the National Oceanic and Atmospheric Administration (NOAA) Profiler Network (NPN; hourly observations). The OM surface pressure variable is modified by adjusting to a constant elevation of 356.6 m (the mean elevation of all OM stations) and subtracting the mean diurnal pressure signal during the calendar month of interest. In addition, virtual temperature observations from NPN stations equipped with a Radio Acoustic Sounding System (RASS) are linearly interpolated to 25-hPa pressure increments in the vertical, and then linearly interpolated in time, to diminish the extent of missing data. Virtual temperature anomalies are calculated by subtracting the mean virtual temperature from the instantaneous observation at each height; the mean is taken over the period during which the MCV (or its parent MCS) is in Oklahoma.

Observations are augmented in the vicinity of each MCV by means of a time–space transformation (Fujita 1951). OM (NPN) observations taken 5 and 10 min (1 h) before and after each time are ''transformed'' from time to space, and plotted along the direction of motion of the MCV. The MCV heading and speed are determined based on level-3 radar imagery from individual Weather Surveillance Radar-1998 Doppler (WSR-88D) stations in Oklahoma. The transformation is applied over a 3°

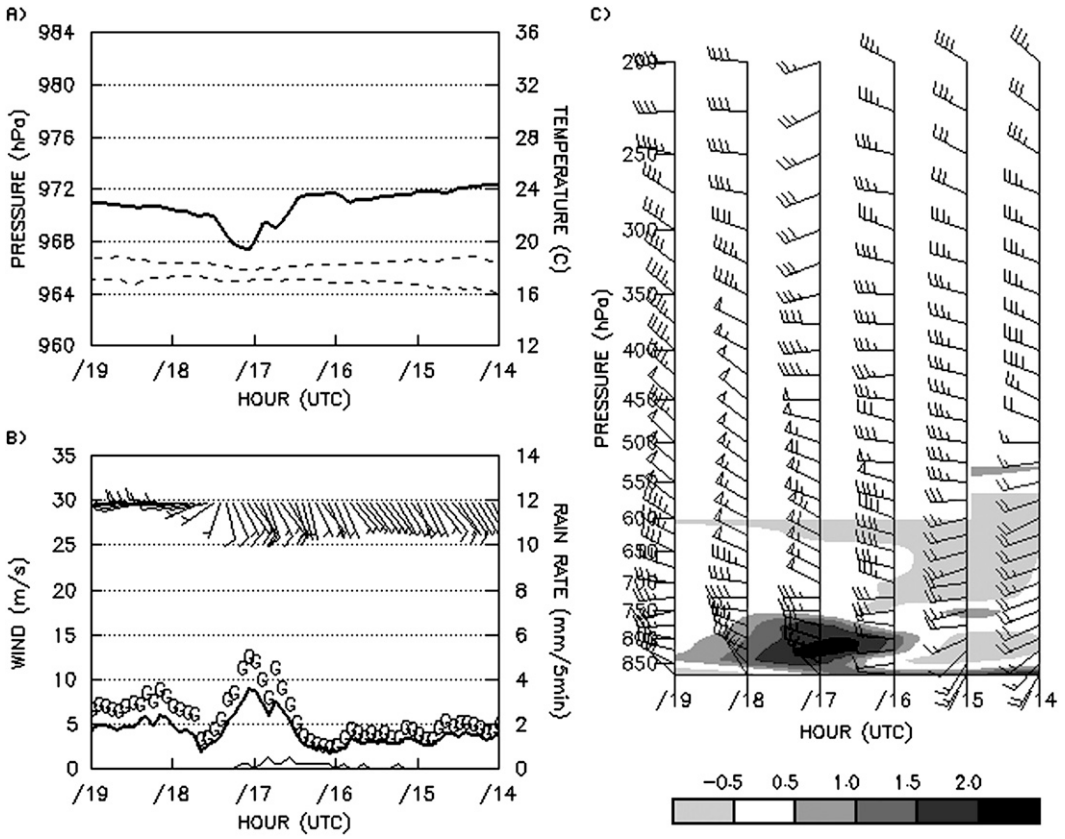

FIG. 3. (a),(b) Meteograms for the Tahlequah OM station (location marked in Fig. 2d) and (c) observed time–height section for the Haskell NPN station (location marked in Fig. 2d), 1400–1900 UTC 24 May 2003. Time runs from right to left. Parameters displayed are (a) surface pressure (hPa; solid line; left axis) adjusted to 356.6-m elevation and 1.5-m air temperature and dew point temperature (°C; dashed lines; right axis); (b) observed 10-m wind barbs (short barb 2.5 m s^{-1}; long barb 5 m s^{-1}), wind speed (m s^{-1}; thick solid line; left axis), wind gusts (m s^{-1}; "G"; left axis), and rainfall [mm (5 min)$^{-1}$; thin solid line; right axis]; and (c) horizontal wind (short barb 2.5 m s^{-1}; long barb 5 m s^{-1}; flag 25 m s^{-1}) and RASS virtual temperature anomalies (°C; shaded, with scale at bottom).

latitude by 3° longitude box centered on the MCV. The size of the box was determined by trial and error, guided by the fact that an MCV might be expected to influence its environment out to a Rossby radius of deformation (about 280 km in a typical MCS environment; Chen and Frank 1993).

Based on these augmented data, detailed analyses of each case are carried out for the period during which the MCV is within the state of Oklahoma. The analyses are undertaken using multiquadratic interpolation (Nuss and Titley 1994) on a 0.1° latitude–longitude grid. The multiquadratic parameter is set to 1.5; the smoothing parameter is set to 5×10^{-6} for OM analyses and 1×10^{-4} for NPN analyses. These values, determined by trial and error, were found to result in the most realistic analyses.

Classification of the MCV cases into repeating types is undertaken based on the behavior of the precipitation structure and the surface pressure field in each case. The following section describes the classification of the 45 Oklahoma MCV cases into 5 recurring types.

3. Results

The dates of each detected MCV case over the period of study, as well as their classification according to the types that are defined in this section, are presented in the appendix. The remainder of this section describes each of the five MCV types, both those producing surface mesolows (three types) and those without surface mesolows (two types), in order of their frequency for each category.

a. Rear-inflow-jet MCV

The most common type of MCV producing a surface mesolow is referred to as the "rear-inflow-jet MCV." This type of MCV composes 19 (42%) of the cases. Table 1 gives the mean characteristics of these MCVs

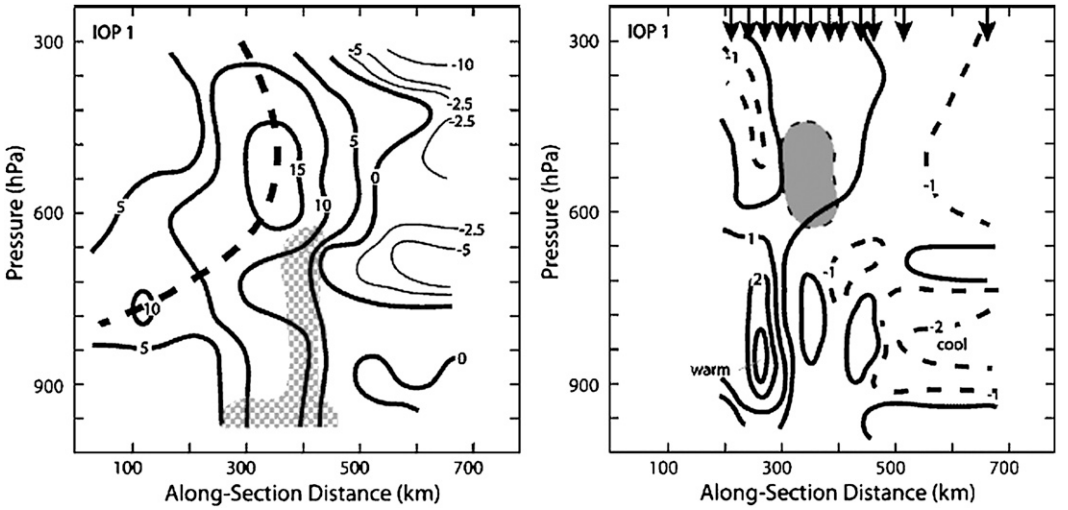

FIG. 4. East–west cross section of BAMEX IOP 1 MCV at 1930 UTC 24 May 2003. (left) Relative vorticity (10^{-5} s^{-1}; contour interval 5×10^{-5} s^{-1} for positive values, 2.5×10^{-5} s^{-1} for negative values), with gray stippling indicating regions where the standard deviation of vorticity exceeds half the maximum value (see details in Davis and Trier 2007), and the heavy dashed line indicating vortex axis. (right) Virtual potential temperature deviations (°C; contour interval 1°C), with gray shading indicating relative vorticity greater than 1.5×10^{-4} s^{-1}, and arrows indicating the locations of soundings projected onto the cross section. [From Davis and Trier (2007).]

compared with the rest of our MCV sample. A one-tailed Student's *t* test reveals that the mean midlevel relative vorticity of rear-inflow-jet MCVs is larger than the mean of the total MCV population; this difference is significant at the 99% level. It is unclear why these MCVs tend to have such strong midlevel relative vorticity compared to the other MCV types.

The MCV of 24–25 May 2003, occurring during the Bow Echo and Mesoscale Convective Vortex Experiment (BAMEX; Davis et al. 2004) campaign, is described in detail here as a representative case of this type of MCV. The parent MCS develops within an environment favorable for deep convection, in moist southeasterly low-level flow (Fig. 1a) near the nose of a weak low-level jet (Fig. 1b), and in the right entrance region of an upper-level jet streak (Fig. 1d) just downstream of a midlevel ridge (Fig. 1c; consistent with the findings of Bartels and Maddox 1991). Figure 2a shows the composite radar reflectivity, surface pressure, and observed 10-m winds at 1400 UTC. There is extensive stratiform rain in northeastern Oklahoma and southeastern Kansas, while on the southwestern side of this there is a small but intense band of convection oriented northeast–southwest. At the surface, there is a well-defined mesohigh on the southwestern end of this convective line. An hour later, at 1500 UTC (Fig. 2b), the convective line has continued to surge southeastward on the western side of the large stratiform region. The reflectivity field shows a developing rear-inflow notch to the north of the convection (marked by a small black arrow), suggesting that a strong RIJ is impinging on the back edge of the stratiform region. The surface pressure field is relatively flat within the MCS, with the exception of the mesohigh at the southwestern end of the convective line. At 1600 UTC (Fig. 2c), the associated MCV is first detected by the objective algorithm; its location is marked with a cross. By this time, the convection is becoming weaker, while the stratiform region is taking on cyclonic curvature. South of the MCV, within the stratiform region, a weak mesolow has appeared. By 1700 UTC (Fig. 2d), the mesolow has become concentrated and deep. The stratiform region appears to be eroded on its back edge to the south of the MCV, and the mesolow is located near the apex of this rear inflow notch.

Figures 3a,b show a meteogram for the Tahlequah, Oklahoma, OM station (location shown in Fig. 2d). The pressure trace shows a very strong and sharp mesolow passing the station at 1705 UTC. The 1.5-m temperature and dew point remain nearly constant and quite close together, indicating high relative humidity. If the mesolow is a hydrostatic phenomenon, as will be argued, the associated temperature perturbations must be confined to regions above the surface in this case. The mesolow passes the station at the same time as the cessation of stratiform rainfall, as noted in several other studies (Johnson and Hamilton 1988; Stumpf et al. 1991).

This case appears very similar to the OK PRE-STORM MCV of 6–7 May 1985, as described by Brandes (1990). That case involved a strong RIJ on the south side of the MCV, leading to a rear-inflow notch with a pronounced

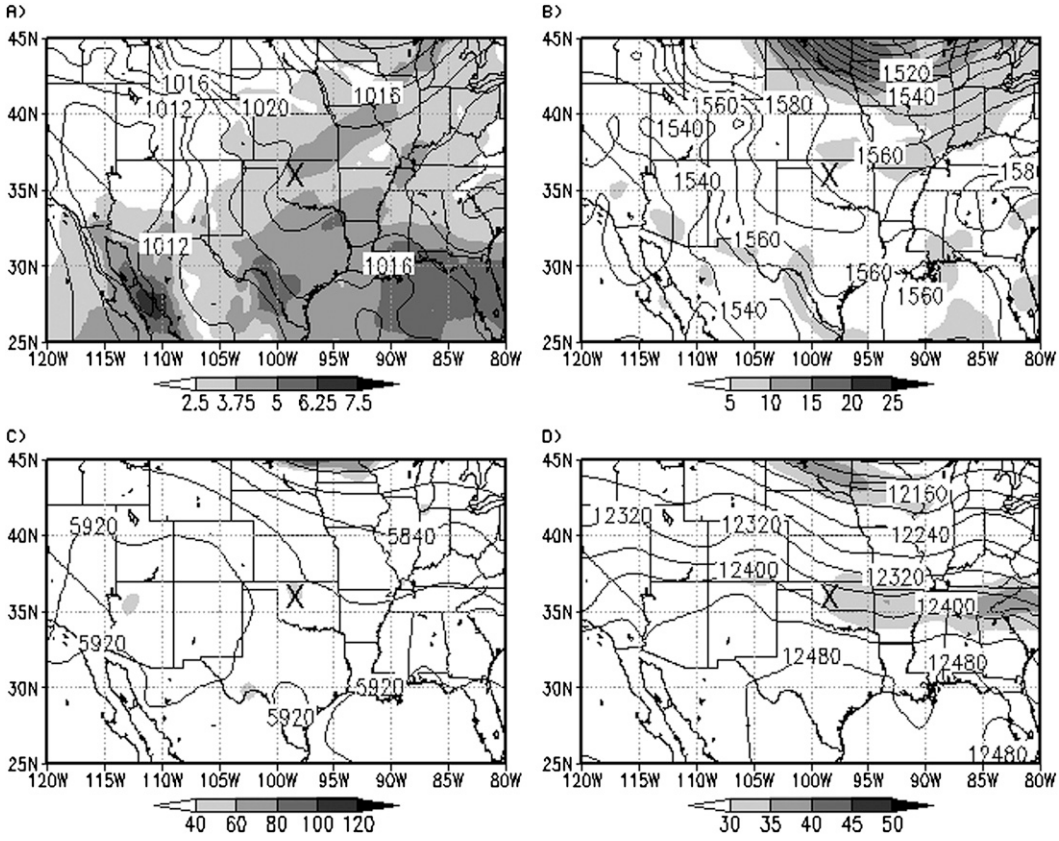

FIG. 5. As in Fig. 1, but at 1200 UTC 9 Aug 2004. (a)–(d) The midlevel MCV center, as detected by the RUC algorithm, is marked by a large cross.

surface mesolow at its apex. Rear-inflow notches have also been documented in other MCV-bearing MCSs (Smull and Houze 1985; Scott and Rutledge 1995; Chong and Bousquet 1999; Knievel and Johnson 2002).

To explain the observed surface pressure features on 24 May 2003 it is necessary to examine the observations aloft. Figure 3c shows a time–height section of observations from the Haskell, Oklahoma, NPN station (location shown in Fig. 2d). The feature of interest is the pronounced low-level virtual warming that occurs over Haskell at 1700 UTC. The virtual temperature anomaly reaches a peak of 2.24°C at 825 hPa; positive anomalies extend up to 750 hPa. This sharp low-level warming is evidently a manifestation of strong subsidence warming associated with a descending RIJ at the back edge of the stratiform precipitation shield. The wind profile at Haskell supports this, with the warming occurring at the base of strong west-northwesterly flow [50 kt (26 m s^{-1}) at 700 hPa]. Note that the core of the jet rises from 600 to 500 hPa during 1700–1900 UTC, consistent with fixed-point observations of a descending jet in an eastward-moving system. Calculation of the hydrostatic pressure change associated with the warming in the Haskell virtual temperature profile from 1500 to 1700 UTC yields a value of −0.87 hPa. The observed change at Okmulgee, Oklahoma, the closest OM station to the Haskell NPN site, over this same time period is −0.79 hPa, suggesting that the low-level warming can explain the entirety of the pressure drop. The significantly larger pressure fall observed at Tahlequah (−3.62 hPa) over this same period suggests that the Haskell profiler did not sample the core of the low-level warming (see Fig. 4).

This MCV was the focus of Intensive Observing Period (IOP) 1 during the BAMEX campaign, and dense aircraft observations were taken during the afternoon of 24 May (Davis and Trier 2007). Figure 4 shows their east–west cross sections of the system, constructed from dropsonde observations and valid at 1930 UTC. The dropsonde observations show a very similar virtual temperature structure to the NPN observations, including a concentrated warm anomaly of more than 3°C centered near 850 hPa. The virtual warmth extends up to 600 hPa and then transitions to a cold anomaly, as in the NPN observations. Also, similar to the NPN observations, a region of virtually cool air is seen a few

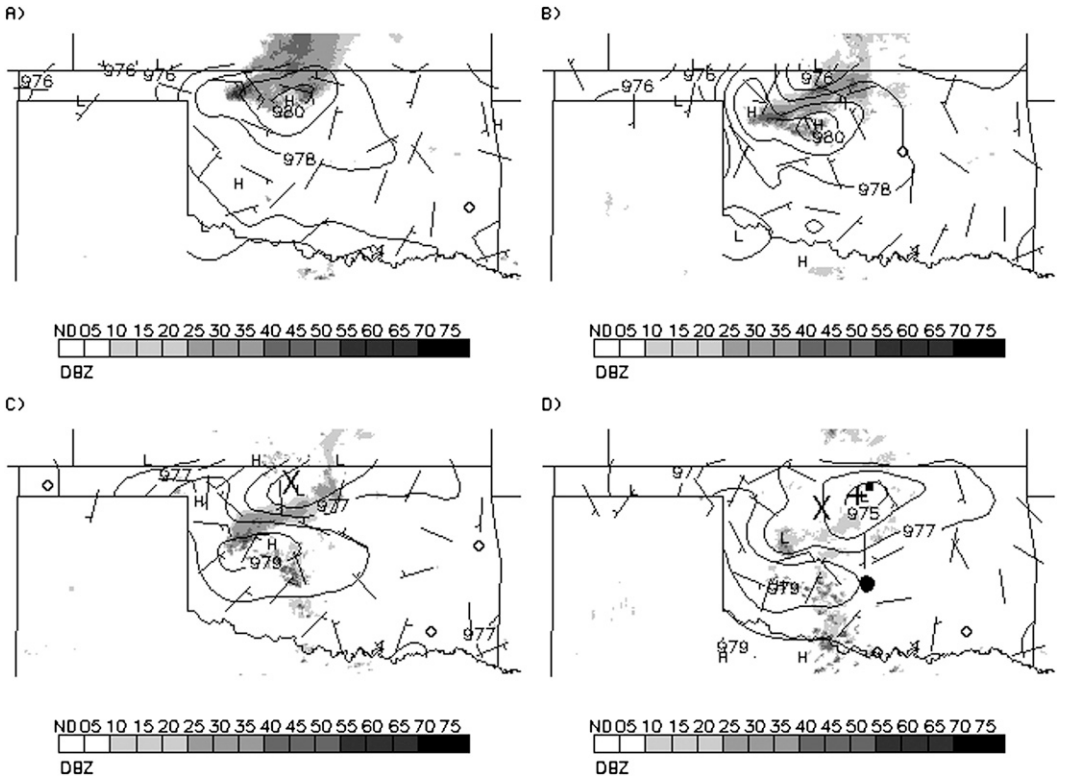

FIG. 6. As in Fig. 2, but at (a) 0800, (b) 0900, (c) 1000, and (d) 1100 UTC 9 Aug 2004. The midlevel MCV center, as detected by the RUC algorithm, is marked by a large cross in (c),(d). The Breckinridge OM station is marked by a plus sign in (d). The Purcell NPN station is marked by a filled circle in (d). The ARM site is marked by a filled square in (d).

hundred kilometers to the east of the warm anomaly, extending over a deep layer except for a small warm pocket near 700 hPa. The extent of the agreement between the two independent datasets is remarkable, and provides confidence in the thermal structure of this MCV. These observations suggest that, in these rear-inflow-jet MCVs, many of which display similar structure (not shown), the small but intense surface mesolow is a reflection of concentrated low-level subsidence warming occurring within a RIJ.

b. Collapsing-stratiform-region MCV

The second type of mesolow-producing MCV observed is termed the ''collapsing-stratiform-region MCV,'' because of the apparent role of the dissipating stratiform region in the development of both the midlevel vortex and a surface mesolow. Eight of these cases are observed during the period of study (18% of the total). The mean radius of collapsing-stratiform-region MCVs is smaller than that of the total MCV population; this difference is significant at the 90% level (Table 1). Similarly, the mean midlevel relative vorticity within collapsing-stratiform-region MCVs is less than the mean of the entire MCV population; this difference is significant at the 95% level. The reduced radius and intensity of these MCVs is likely related to the small size of the parent MCSs; these MCSs are anomalously small even at maturity.

The typical evolution of collapsing-stratiform-region MCVs is illustrated with one of the cases documented here, occurring on 9–10 August 2004. Figure 5 depicts the environment near the time of MCV formation; by this time the parent MCS is dissipating within a region of northwesterly upper-level flow (Fig. 5d) and weak low- to midlevel flow (Figs. 5a–c), once again in proximity to an upper-level ridge (Bartels and Maddox 1991). Figure 6a shows the parent MCS at 0800 UTC, as it enters northwestern Oklahoma. The radar reflectivity shows a stratiform region centered just north of the Kansas–Oklahoma border, with a mesohigh at the southern fringe of the precipitation. An hour later (Fig. 6b), the stratiform region is in the process of dissipating, and the mesohigh has moved farther south, while a pronounced pressure gradient is beginning to appear within the southern portion of the dissipating precipitation shield. By 1000 UTC (Fig. 6c), the mesohigh is centered south of the remaining rain area, and a broad mesolow has

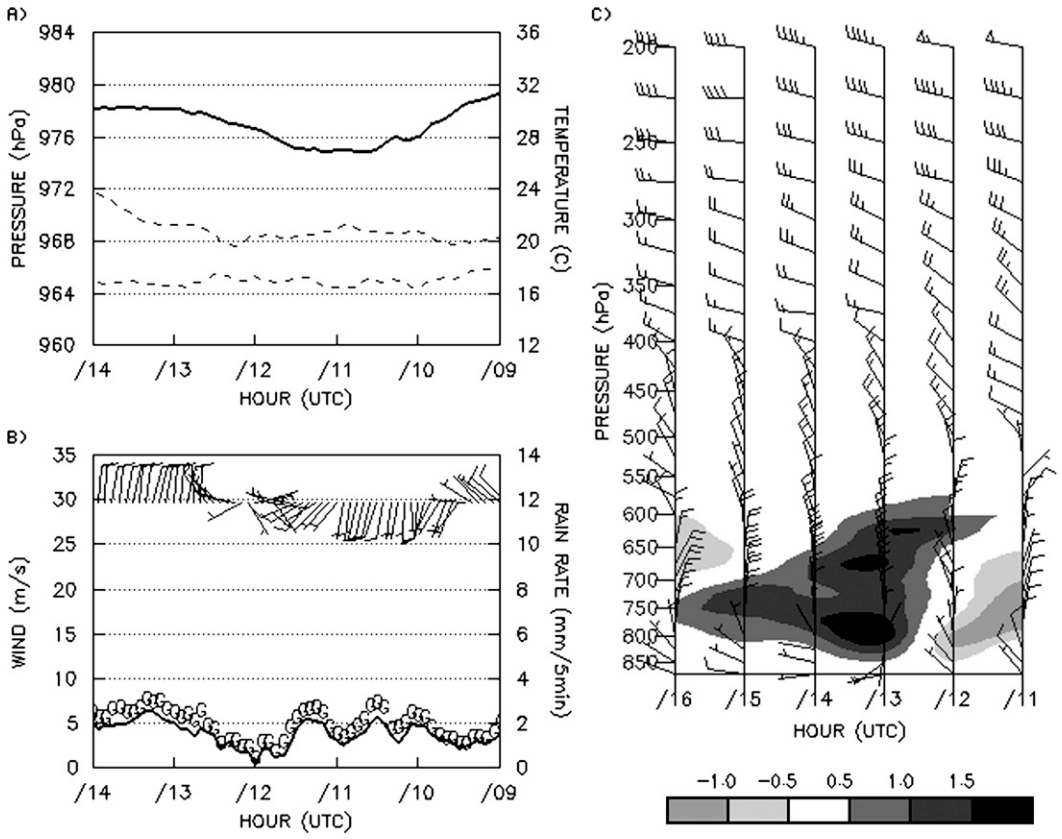

FIG. 7. As in Fig. 3, but (a),(b) for the Breckinridge OM station (location marked in Fig. 6d), 0900–1400 UTC, and (c) for the Purcell NPN station (location marked in Fig. 6d), 1100–1600 UTC 9 Aug 2004.

developed to its north. The MCV associated with the system is first detected by the objective algorithm at this time, located directly over the southern portion of the mesolow. By 1100 UTC (Fig. 6d), the stratiform precipitation has nearly dissipated, leaving a large and relatively deep mesolow centered in northern Oklahoma and a weakening mesohigh to its south.

Figures 7a,b show a meteogram for the Breckinridge, Oklahoma, OM station (location marked in Fig. 6d). The pressure trace shows the passage of a well-defined mesolow of 4-hPa amplitude, lasting 3 h with a minimum pressure near 1100 UTC. While the magnitude of the pressure gradient between the mesohigh and mesolow is fairly significant [6 hPa (100 km)$^{-1}$], the observed winds at the surrounding OM stations remain quite low. This is presumably due to the transient and unbalanced nature of the pressure field (Vescio and Johnson 1992). Another notable feature of Fig. 7a is the minimal temperature and dew point variations during the passage of the mesolow. The evolution of the 9–10 August 2004 case appears very similar to that of the 23–24 June 1985 OK PRE-STORM MCS, examined by Johnson et al. (1989).

Once again, in order to investigate the causes of the surface pressure features associated with collapsing-stratiform-region MCVs, it is necessary to look above the surface. Figure 7c shows a time series of observations from the Purcell, Oklahoma, NPN station (location marked in Fig. 6d) during the 9–10 August 2004 case. Note that the Purcell station is located in south-central Oklahoma; thus the mesolow does not move overhead until 1300 UTC, and is weaker by this time (not shown). Around the same time as mesolow passage, the RASS virtual temperature anomalies exhibit a broad and deep maximum. The warm anomaly extends from 850 hPa to near the top of the RASS measurements (575 hPa). The anomaly lasts several hours, and reaches a maximum of 1.88°C. Direct calculation of the hydrostatic pressure change associated with the change in the RASS virtual temperature profile from 1100 to 1300 UTC below 600 hPa gives a value of −1.75 hPa. The observed pressure drop at Washington, Oklahoma, the nearest OM station to Purcell, is 1.52 hPa over the same 2-h period. This suggests (assuming no compensating temperature changes aloft) that the warming observed below 600 hPa can explain the entirety of the pressure fall.

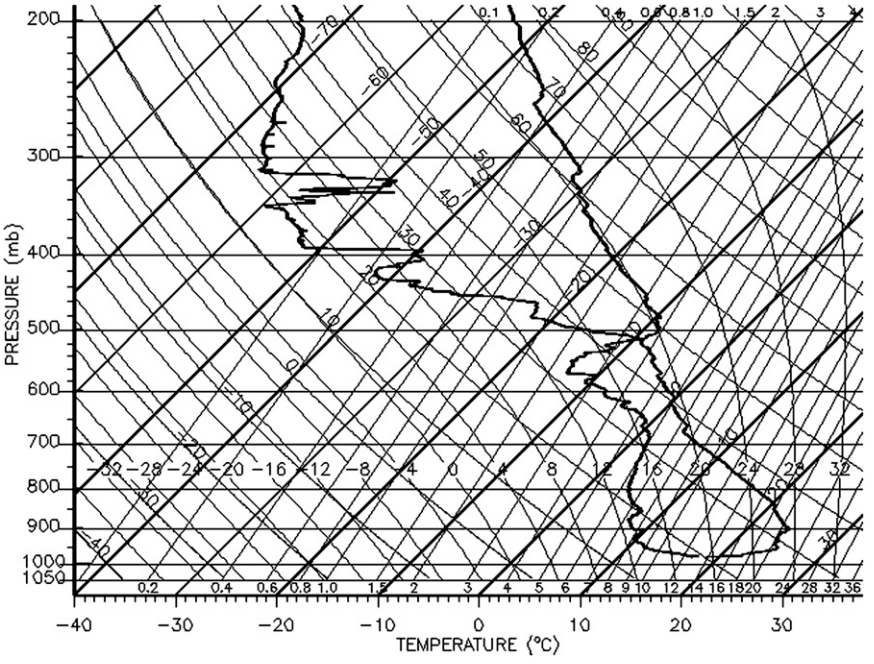

FIG. 8. Skew T–log$p$ plot of radiosonde from the Oklahoma ARM site (location marked in Fig. 6d) at 1136 UTC 9 Aug 2004. Right-hand trace is temperature (°C), and left-hand trace is dew point temperature (°C).

It seems probable that this virtual warmth is a result of broad subsidence warming, which could occur within the dissipating remnants of an MCS. After the dissipation of all the precipitation within the MCS stratiform region, continuing descent would produce adiabatic warming within a stably stratified atmosphere. Support for this hypothesis is presented in Fig. 8, which shows a skew T–log$p$ diagram of a radiosonde launched from the Atmospheric Radiation Measurement (ARM) site in northern Oklahoma (location shown in Fig. 6d) at 1136 UTC. Above a low-level nocturnal inversion, there is a deep dry-adiabatic layer up to above 700 hPa. This dry-adiabatic layer resembles the ''onion'' soundings documented by Zipser (1977) in the trailing stratiform regions of tropical MCSs. At this time of day, this layer likely represents a region of subsidence warming, especially considering the absence of any such well-mixed layer in the 1200 UTC soundings at Norman, Oklahoma; Dodge City, Kansas; or Amarillo, Texas.

Taken together, these observations strongly suggest that the well-defined mesolows observed in collapsing-stratiform-region MCVs are due to broad low- to midlevel subsidence warming occurring within the dissipating stratiform regions of MCSs. The frequent close proximity of the surface mesolow and midlevel vortex suggests there could be a dynamical link between the two. From the perspective of the vorticity equation, low- to midlevel subsidence, such as that producing the mesolows in these systems, would contribute to a spinup of vorticity by the stretching term. In a favorable environment of weak cyclonic vorticity, this contribution could be a major factor in MCV formation and amplification at low levels.

c. *Vertically coherent MCV*

The third kind of MCV producing a surface mesolow is termed the ''vertically coherent MCV.'' Only one of the cases documented here displays this behavior: that of 29 July 2004. This appears to be the only case where the midlevel vortex produces a genuine reflection in the surface wind field (i.e., an associated low-level vortex). This MCV has a larger radius than the mean of the total population (Table 1).

The MCV forms in a rather moist environment in northern Texas (Fig. 9a), on the cyclonic shear side of a low-level jet (LLJ; Fig. 9b) and just ahead of a mid- to upper-level shortwave trough (Figs. 9c,d); this environment would support synoptic-scale ascent in the region. The MCV's positioning with respect to the LLJ is also conducive to heavy rainfall (Schumacher and Johnson 2009). The flow configuration in this case differs from the archetypal pattern of MCV formation within an upper-level ridge. The distinguishing feature of this MCV is the persistent and relatively large-scale surface mesolow attendant to the midlevel circulation. Figure 10a

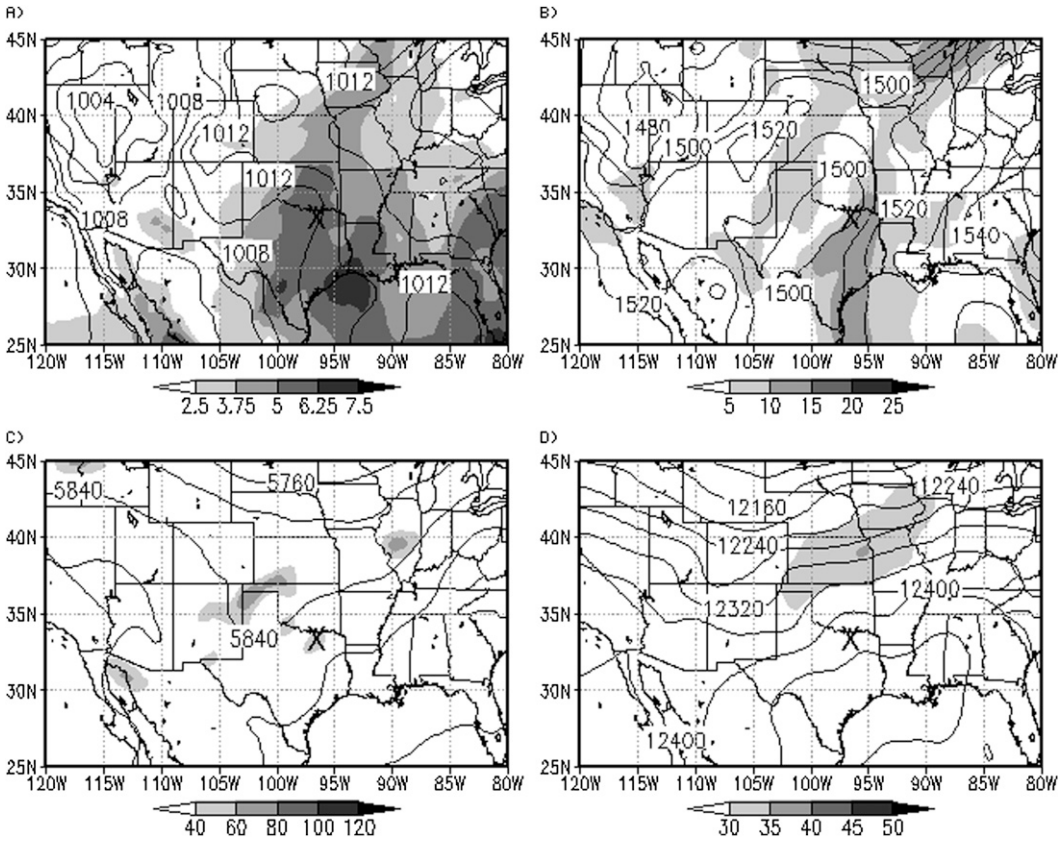

FIG. 9. As in Fig. 1, but at 1200 UTC 29 Jul 2004. (a)–(d) The location of the developing MCV is marked by a large cross.

shows the precipitation structure and surface pressure field at 1300 UTC 29 July 2004. The midlevel MCV center is just south of the analysis domain at this time. There is widespread light to moderate stratiform precipitation within the MCV's circulation. The pressure field shows a large and broad mesolow just southwest of the precipitation shield. An hour later (Fig. 10b), the mesolow has consolidated, and the entire rain shield is rotating cyclonically around the mesolow; this rotation is clearly seen when successive 15-min radar images are animated on the computer screen. During 1500–1600 UTC (Figs. 10c,d), the system continues to drift slowly northeastward through Oklahoma, with the mesolow remaining strong. It should be noted that, throughout the analysis period, the observed surface winds, although light, form a closed cyclonic circulation centered on the mesolow.

The surface weather effects of this MCV can be seen in the meteogram for the mesonet station at McAlester, Oklahoma (location shown in Fig. 10d), displayed in Figs. 11a,b. The pressure trace reveals that the mesolow is very broad and shallow; the pressure fall is only about 2 hPa, but commences hours before the lowest pressure is observed (1630 UTC). The near-surface air is very nearly saturated, with dew point depressions of <1°C much of the time. The MCV occurs within a north–south temperature gradient, with the temperature rising 4°C over 2 h; this temperature gradient seems to be associated with a weak surface warm front. While the winds clearly show the passage of a cyclonic circulation near 1630 UTC, the speeds remain generally below 5 m s^{-1}.

Figure 11c shows a time–height section of NPN observations from the station at Purcell (location shown in Fig. 10d). The weakness of the virtual temperature anomalies in this case is notable; the warmest anomaly observed is only 0.7°C (650 hPa, 1500 UTC). Figure 12 shows a north–south cross section of PV through the MCV center at 1200 UTC, based on the RUC analysis. The MCV is represented as a large and relatively deep PV tower, nearly vertically aligned. The PV tower appears directly over the surface mesolow (location marked in Fig. 12), which is itself embedded within the surface frontal zone. Potential vorticity of $>10^{-6}$ K m^2 kg^{-1} s^{-1} extends up to nearly 450 hPa, and the PV tower is about 200 km in diameter. The isentropes, overlaid on the PV field in Fig. 12, are slightly depressed within the PV tower from 800 to 500 hPa; this warm core does not appear to

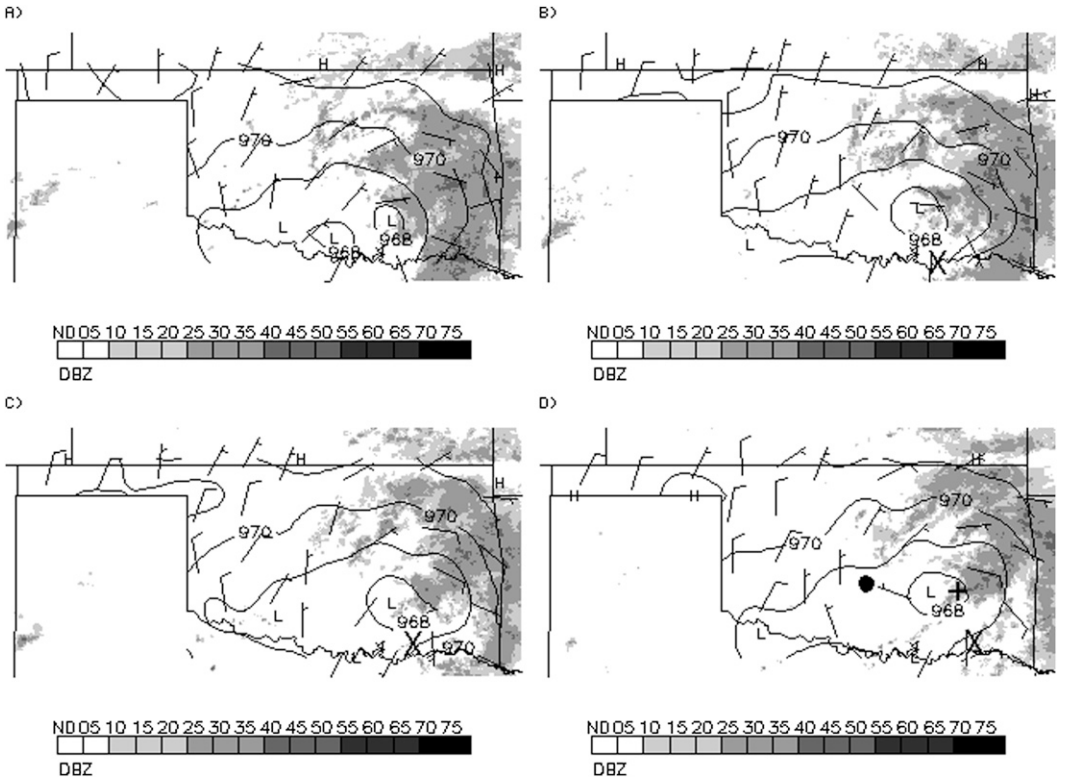

FIG. 10. As in Fig. 2, but at (a) 1300, (b) 1400, (c) 1500, and (d) 1600 UTC 29 Jul 2004. The midlevel MCV center, as detected by the RUC algorithm, is marked by a large cross in (b)–(d). The McAlester OM station is marked by a plus sign in (d). The Purcell NPN station is marked by a filled circle in (d).

penetrate to the surface. There is no negative PV anomaly overlying the PV tower as has been reported in other MCVs (e.g., Fritsch et al. 1994).

An examination of the BAMEX MCV cases discussed by Davis and Trier (2007) reveals a very similar MCV to the present case, occurring during IOP 8 on 11 June 2003. Figure 13 shows east–west cross sections of this MCV, in terms of relative vorticity and virtual potential temperature anomaly. The relative vorticity cross section shows a coherent and vertically stacked vortex, with strong vorticity ($>1.5 \times 10^{-4}$ s^{-1}) extending up to 400 hPa. While relative vorticity is not equivalent to PV, the shape and depth of the relative vorticity maximum is remarkably similar to the PV tower seen in the 29 July 2004 case (Fig. 12). Another similarity emerges in the right-hand panel of Fig. 13, which shows that the virtual potential temperature deviations in the vicinity of this BAMEX MCV are minimal. The occurrence of such an MCV during the BAMEX campaign, displaying such marked similarities to the case documented here, supports the classification of these MCVs in their own category.

The question arises as to what mechanism is responsible for the development of low pressure at the surface in vertically coherent MCVs. The vertical coherence of the PV anomaly in these cases, as well as the proximity of the surface mesolow to the center of the PV tower, suggests that the mesolow may be due to a developing, deep warm core within the MCV. Such a warm core could be produced by the diabatic heating occurring within the persistent precipitation shield in the vicinity of the MCV. In the 29 July 2004 case, the precipitation shield itself, occurring on the east side of the vortex, is likely due to the balanced lifting mechanism proposed by Raymond and Jiang (1990) acting on the north–south temperature gradient associated with the warm front. The extension of the MCV to the surface in these cases is likely enabled by the relative lack of a surface-based cold pool because of the very moist environment; according to the RUC analyses, the precipitable water in the vicinity of the vortex remains well above 5 cm (Fig. 9a). This mechanism of surface low development due to the strengthening and deepening of a warm core has been documented in prior studies of MCVs (Fritsch et al. 1994; Rogers and Fritsch 2001; Trier and Davis 2002; Davis and Galarneau 2009). The low-level cyclonic vorticity maximum would develop in response to the presence of a surface mesolow.

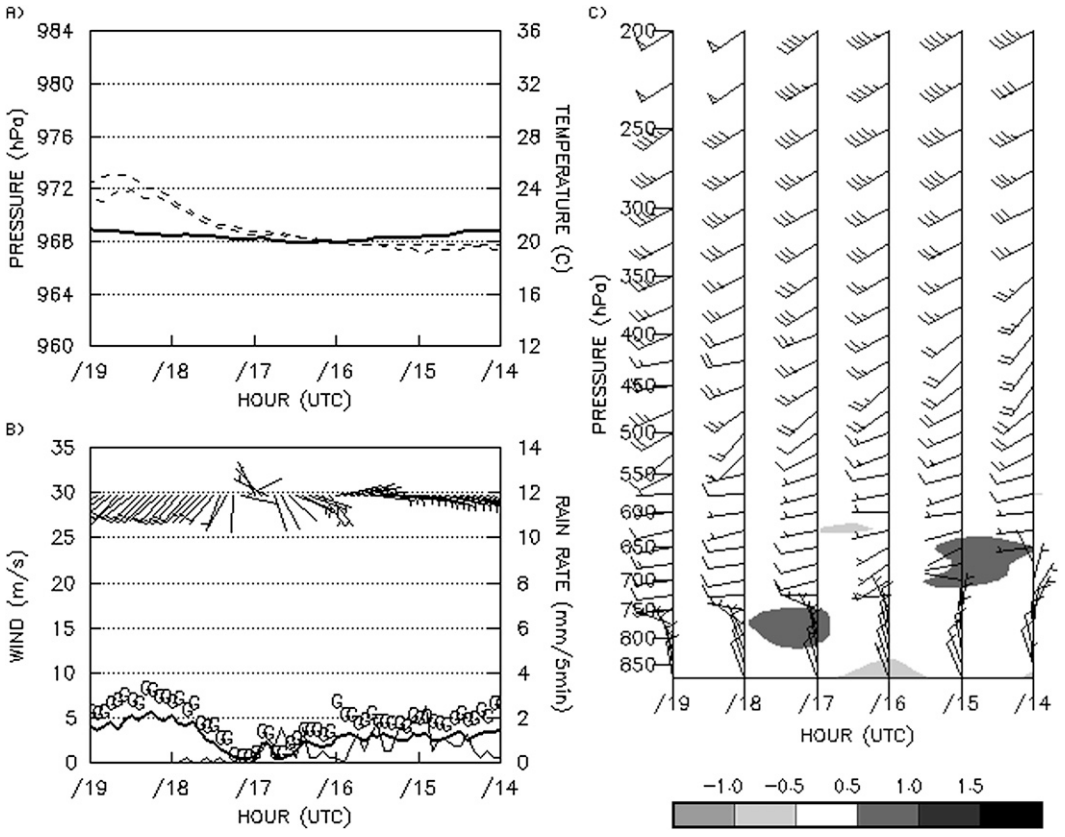

FIG. 11. As in Fig. 3, but (a),(b) for the McAlester OM station (location marked in Fig. 10d) and (c) for the Purcell NPN station (location marked in Fig. 10d), 1400–1900 UTC 29 Jul 2004.

d. Remnant-circulation MCV

The most common type of MCV without a surface mesolow is called the ''remnant-circulation MCV.'' This type of MCV evolution appears to be fairly common; 14 of the 45 cases studied herein (31%) display this behavior (Table 1). These cases are marked by a lack of precipitation in the vicinity of the MCV, as well as the absence of a surface mesolow.

One of these remnant-circulation MCVs occurred on 20–21 June 2003, and is representative of this type of MCV. This MCV forms from a dissipating MCS in a relatively moist environment (Fig. 14a) south of a LLJ (Fig. 14b), near the crest of a mid- to upper-level ridge (Figs. 14c,d). By the time the MCV enters Oklahoma at 1500 UTC (Fig. 15a), very little remains of the precipitation related to the parent MCS. The surface pressure gradient is weak, and over the next 3 h (Figs. 15b–d) there is little change. During this time, the MCV moves slowly southeastward through western Oklahoma, but there is no trace of the vortex at the surface. What appears to be a weak mesolow is likely only an effect of the analysis domain edge. Figures 16a,b show surface

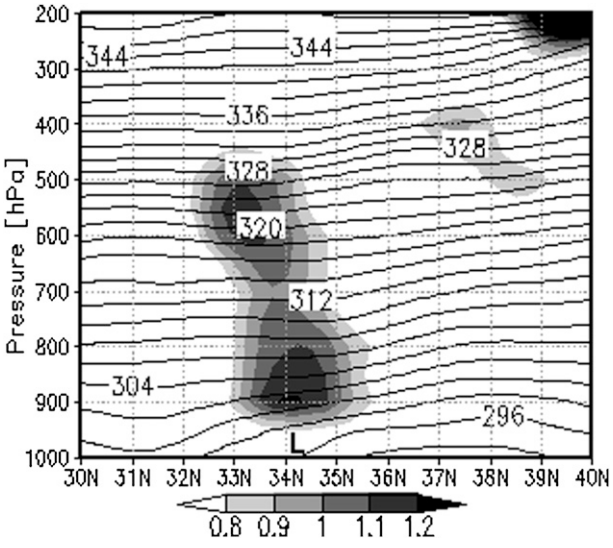

FIG. 12. RUC analysis of potential temperature (K; contour interval 2 K) and PV (10^{-6} K m^2 kg^{-1} s^{-1}; shaded, with scale at bottom) along vertical section at 96.75°W at 1200 UTC 29 Jul 2004. The mesolow location is marked by an ''L'' on the lower axis.

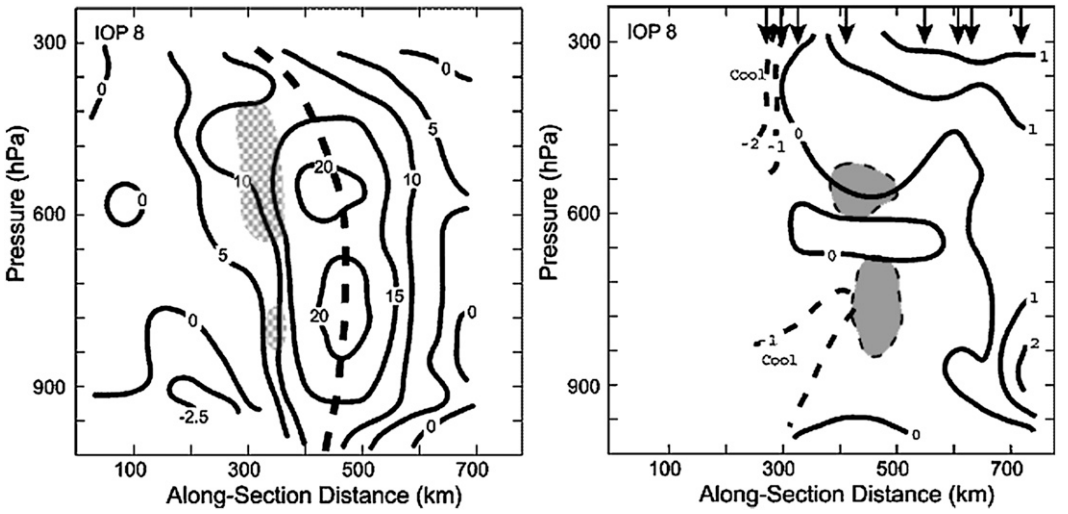

FIG. 13. As in Fig. 4, but of BAMEX IOP 8 MCV at 1730 UTC 11 Jun 2003. (right) The gray shading indicates relative vorticity greater than 2×10^{-4} s^{-1}. [From Davis and Trier (2007).]

observations from the Camargo, Oklahoma, OM station (location shown in Fig. 15d). There is no evidence of a precipitation-induced cold pool in any of the variables, which display a normal diurnal cycle. Similarly, RASS virtual temperature observations (Fig. 16c) show only weak temperature perturbations. This case is representative of many of this type of MCV. It appears that the development of a surface mesolow associated with an

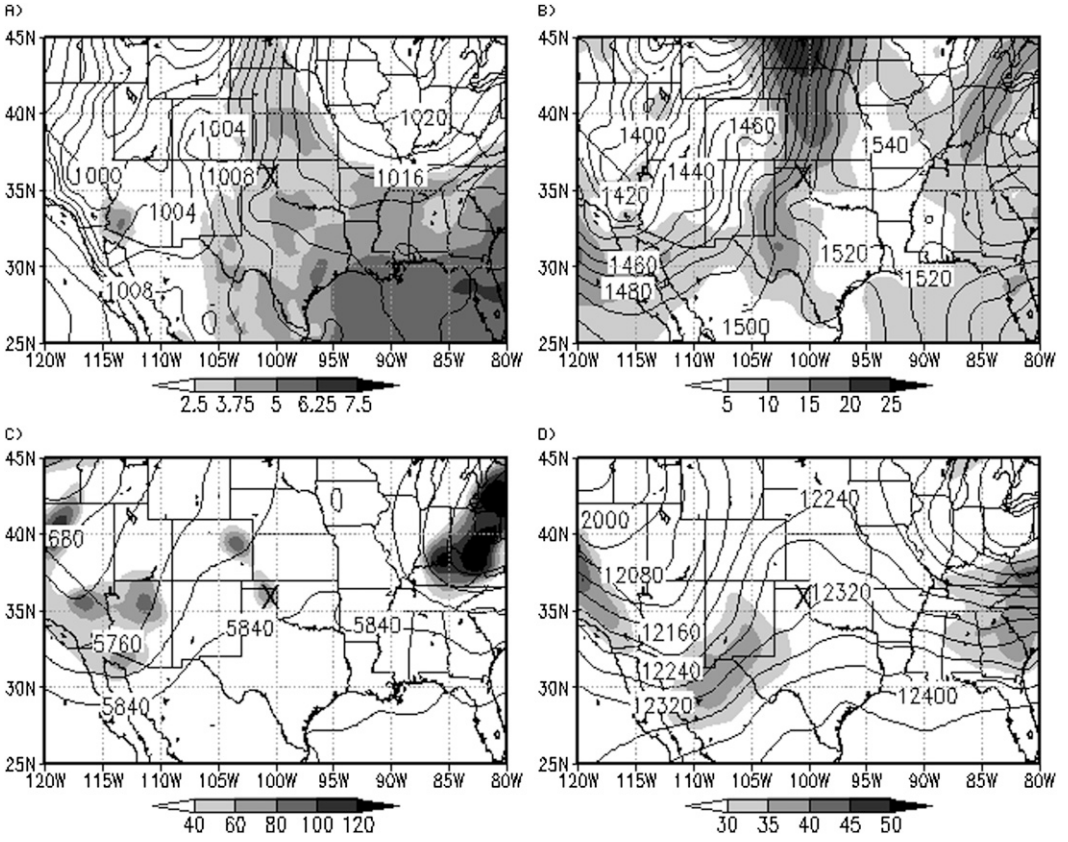

FIG. 14. As in Fig. 1, but at 1200 UTC 20 Jun 2003. (a)–(d) The midlevel MCV center, as detected by the RUC algorithm, is marked by a large cross.

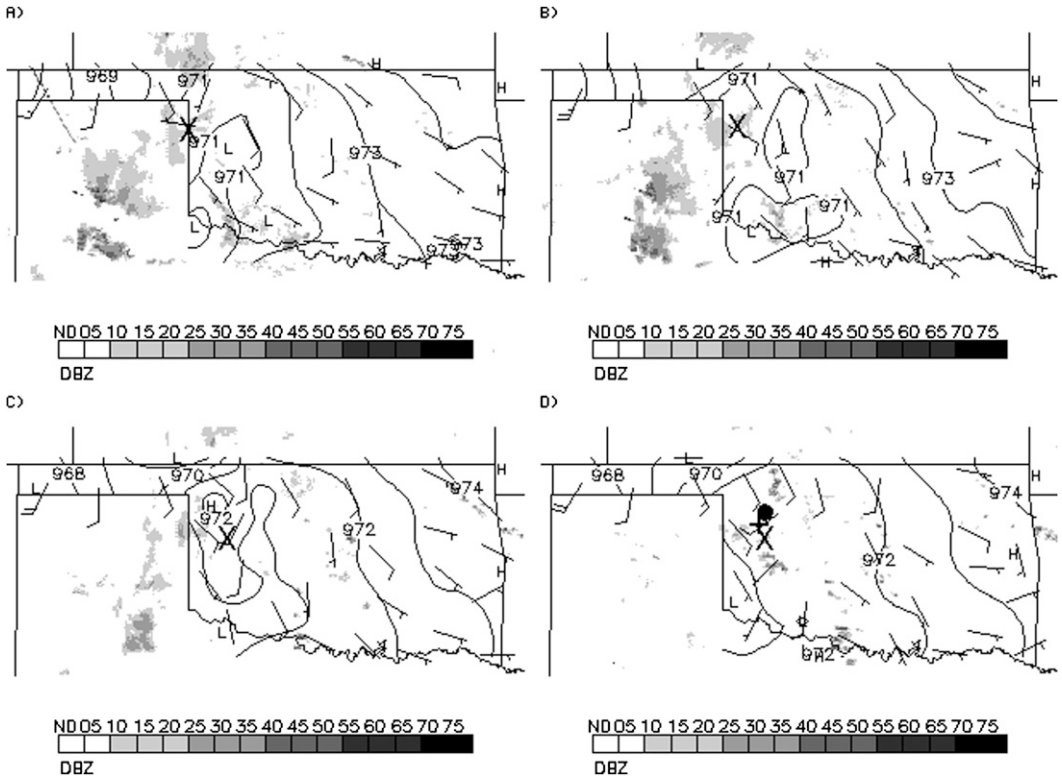

FIG. 15. As in Fig. 2, but at (a) 1500, (b) 1600, (c) 1700, and (d) 1800 UTC 20 Jun 2003. The midlevel MCV center, as detected by the RUC algorithm, is marked by a large cross in (a)–(d). The Camargo OM station is marked by a plus sign in (d). The Vici NPN station is marked by a filled circle in (d).

MCV requires at least some precipitation in the vicinity of the vortex. Without this precipitation, there will not be strong subsidence to generate warming in unsaturated downdrafts (such as seen in the collapsing-stratiform-region and rear-inflow-jet MCVs), nor will there be diabatic heating to generate a deep warm core (as seen in the vertically coherent MCV).

e. Cold-pool-dominated MCV

The less common type of MCV without a surface mesolow is termed the ''cold-pool-dominated MCV''. Three of these MCVs (7% of the total population) are documented in Oklahoma during the period of study (Table 1). The distinguishing feature of these cases is the presence of an active MCS during part of the MCV lifetime, but the absence of any significant surface mesolow.

The evolution of these cases is illustrated here based on a representative case from 30 July 2003. The MCS that produces this MCV initiates in southeastern Wyoming in the late morning of 29 July. The MCV formation occurs in northwesterly flow aloft (Figs. 17c,d) and weak flow at low levels (Figs. 17a,b), once again in the typical flow pattern conducive to MCV genesis (Bartels and Maddox 1991). Figure 18a shows the radar reflectivity and surface pressure field at 1100 UTC. The pressure gradients are weak; the main feature is the mesohigh centered within the stratiform region. Two hours later (Fig. 18b), the MCV continues slowly moving through northern Oklahoma, and the surface pressure field remains nondescript; this is likely due to the presence of widespread low-level cool air. During the next few hours (Figs. 18c,d), the convection weakens, followed by the dissipation of the stratiform precipitation. Figures 19a,b show a meteogram from the Lahoma, Oklahoma, OM station (location shown in Fig. 18d). During 0900–1200 UTC, while the MCV moves nearly overhead, the surface air is cool and nearly saturated, with slightly elevated pressure. This air mass is much colder than that observed earlier in the analysis period (before 0800 UTC). Profiler observations (Fig. 19c) reveal that the cold pool extends up to the midtroposphere; no warm anomalies are detected above this. The presence of a surface-based cold pool in these cases acts to raise the surface pressure hydrostatically; it also restricts the downward development of the warm core within the MCS, which is another possible mechanism for mesolow formation.

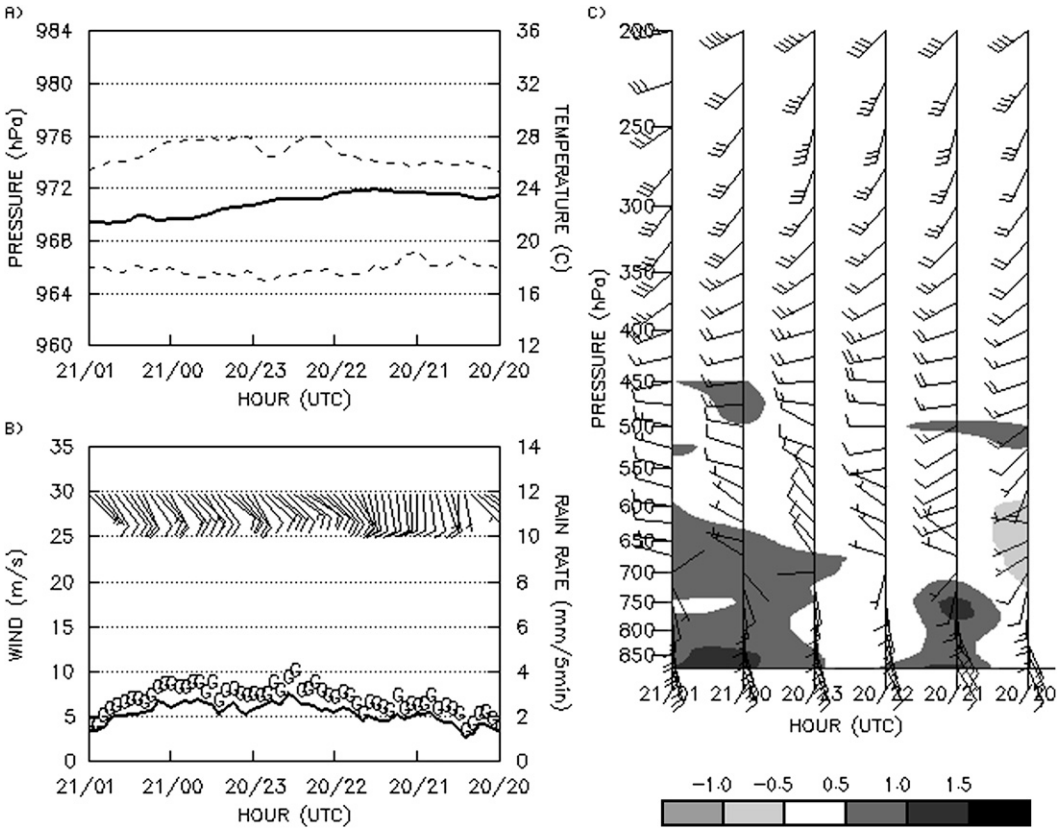

FIG. 16. As in Fig. 3, but (a),(b) for the Camargo OM station (location marked in Fig. 15d) and (c) for the Vici NPN station (location marked in Fig. 15d), 2000 UTC 20 Jun–0100 UTC 21 Jun 2003.

4. Discussion

This study classifies MCVs into several types involving recurring patterns of organization and surface effects. The majority of the MCVs documented herein develop within generally weak midlevel flow in proximity to an upper-level ridge, consistent with the characteristic MCV flow environment identified by Bartels and Maddox (1991). The remainder of this section reviews the five types, and presents conceptual models of two of the three MCV types containing significant surface mesolows. Only one vertically coherent MCV was observed; thus, despite its many interesting features and potential relevance to tropical cyclogenesis, we do not attempt to develop a conceptual model of this MCV type.

Rear-inflow-jet MCVs (19 of the 45 cases, or 42% of total) are the most frequent MCV type containing a marked surface mesolow. In these cases, the development of low surface pressure seems to occur because of the well-documented wake low mechanism, whereby a RIJ flowing into an MCS stratiform region descends strongly, producing a concentrated region of subsidence warming at low levels where the precipitation has evaporated (Johnson and Hamilton 1988). Figure 20 shows a conceptual diagram of the evolution of these MCVs. The left panel represents the mature stage of the parent MCS. These MCSs show a variety of organizations, but one of the most frequent is the leading-line/trailing-stratiform MCS (Houze et al. 1990). The surface pressure field at this time consists of a broad mesohigh within the precipitation. The middle panel of Fig. 20 shows a later stage of development; by this time, the precipitation structure is starting to develop asymmetry, with the right-hand portion of the stratiform region (relative to the system motion) eroding because of the development of the rear inflow on this side of the incipient MCV. A small mesolow appears behind this eroded portion of the stratiform region. On average, the MCV is first detected by the objective algorithm near this time. The specific location of the MCS mesohigh varies considerably among the cases, but in the mean the highest pressure is located in the left-hand portion of the precipitation region relative to system motion. At the final stage, depicted in the right panel of Fig. 20, the stratiform region has been largely shunted to the left of the system motion. The MCV is intensifying in the remaining portion of the

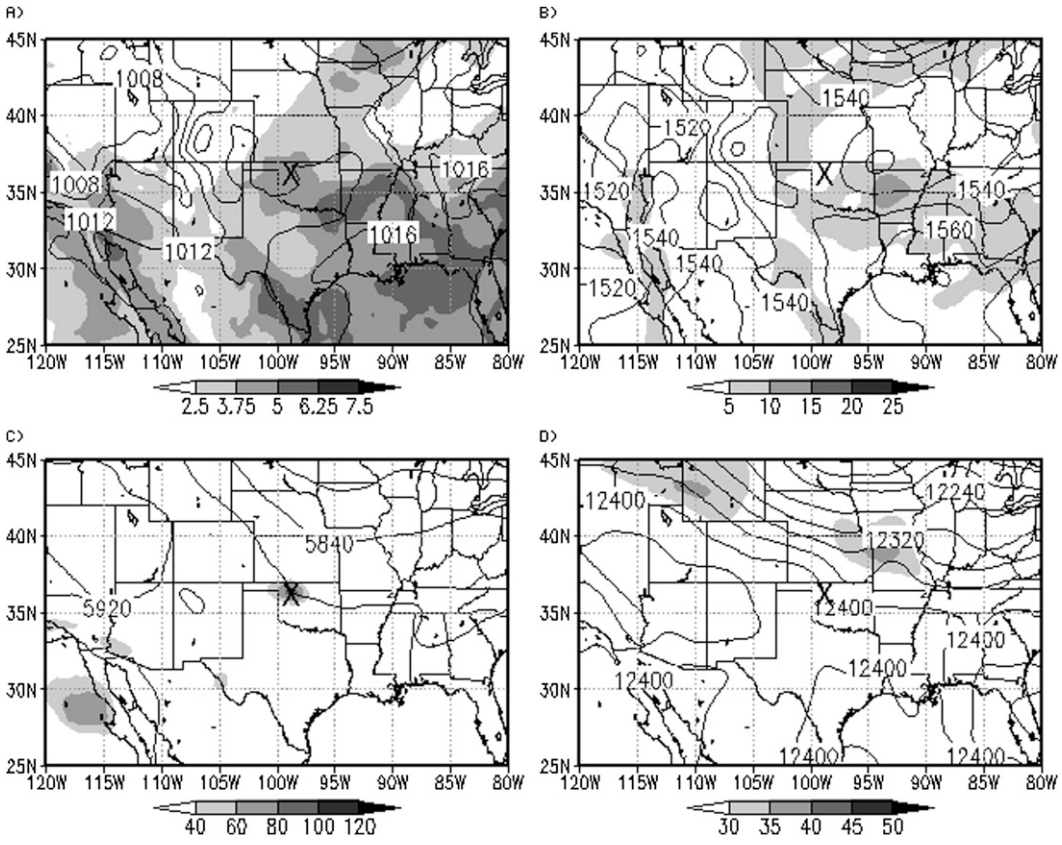

FIG. 17. As in Fig. 1, but at 1200 UTC 30 Jul 2003. (a)–(d) The midlevel MCV center, as detected by the RUC algorithm, is marked by a large cross.

stratiform region, and a concentrated and intense mesolow has formed just behind the eroded portion of the stratiform region.

The organization of many of these rear-inflow-jet MCVs (and, to a lesser extent, that of the collapsing-stratiform-region MCVs) strongly resembles an asymmetric squall line (Houze et al. 1990), but with an embedded MCV in the northern portion of the system, as introduced by Houze et al. (1989, their Fig. 2b). A similar asymmetric precipitation structure has been documented among the OK PRE-STORM MCSs by Loehrer and Johnson (1995, see their Fig. 22b), but with a mesolow occurring behind the trailing stratiform region on the north side of the system rather than on the south side. Mesolows do occur in this position in two of the MCVs examined here; these MCVs are classified as rear-inflow-jet MCVs because of the positioning of the mesolow just behind the stratiform precipitation. This subset of rear-inflow-jet MCVs may have distinct features, and merits further study.

The role of the MCV in these rear-inflow-jet MCVs is somewhat obscure; perhaps it influences the positioning and strength of the rear inflow. Brandes (1990) argued that the MCV within the 6–7 May 1985 OK PRE-STORM MCS enhanced the rear inflow on its southern side; this MCV displayed many similarities to the rear-inflow-jet MCVs described here. In that case, as well as in the cases documented here, the location of the mesolow appears to be determined by the location of the RIJ with respect to the stratiform region.

The eight collapsing-stratiform-region MCVs (18% of the MCVs) display the least variation in structure of all the MCV types. Figure 21 shows a conceptual model of the evolution of the collapsing-stratiform-region MCV. The left panel represents the mature stage of the parent MCS; these MCSs often display a very specific organization consisting of a weak convective line (variably oriented, but on average shifted 45° relative to the direction of motion) with a small stratiform region to the left of the system motion. This is similar to the ''parallel stratiform'' organization of Parker and Johnson (2000), but the convection is not always linear or oriented perpendicular to system motion. At this stage, the surface pressure field is characterized by a mesohigh within the convective region. The central panel of Fig. 21 shows an intermediate stage in the evolution of the system, by

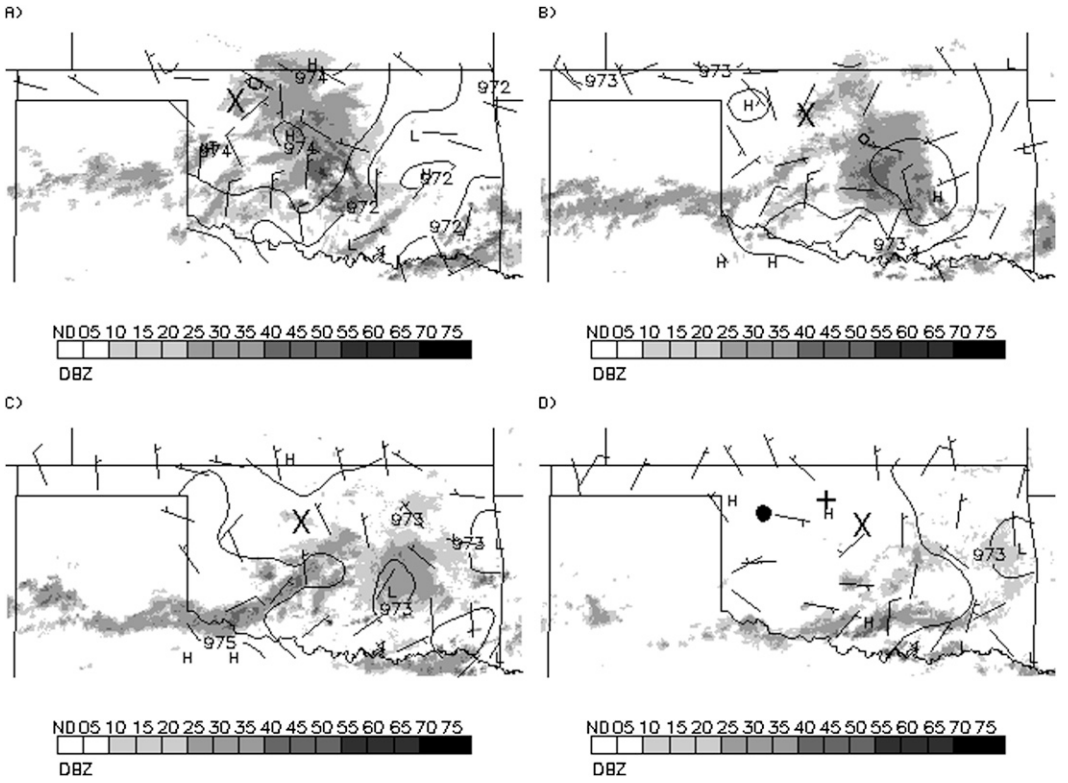

FIG. 18. As in Fig. 2, but at (a) 1100, (b) 1300, (c) 1500, and (d) 1700 UTC 30 Jul 2003. The midlevel MCV center, as detected by the RUC algorithm, is marked by a large cross in (a)–(d). The Lahoma OM station is marked by a plus sign in (d). The Vici NPN station is marked by a filled circle in (d).

which time the convection is weakening, the stratiform region is beginning to dissipate, a small mesolow appears at the rear of the stratiform region, and the surface mesohigh is beginning to move out ahead of the precipitation and weaken. The midlevel vortex generally becomes sufficiently intense to be first detected by the objective algorithm a few hours after this time. The right panel in Fig. 21 shows the final stage in the evolution of these MCVs; the broadening and deepening mesolow has moved into the dissipating remnants of the stratiform region, and the weak mesohigh has moved farther ahead. The formation of both the MCV and the surface mesolow occurs during the weakening stage of the parent MCS.

It was noted in section 3b that collapsing-stratiform-region MCVs tend to be smaller and weaker than other MCVs. These characteristics are a possible explanation for the lack of RIJs and associated wake lows within these MCVs. Regarding the movement of the mesohigh out ahead of the precipitation, similar behavior has recently been observed associated with bowing line segments in linear MCSs (Adams-Selin and Johnson 2010). It is not clear whether the same mechanisms are acting in these collapsing-stratiform-region MCVs. We do note that there is very little temperature perturbation associated with these mesohighs, which suggests a gravity wave mechanism rather than a density current mechanism. The surface mesolow appears at least indirectly related to the development of the MCV: it is likely that both develop as a result of relatively deep low- to midlevel subsidence. This subsidence is driven by the dissipation of the stratiform precipitation and the associated collapsing and spreading of the surface-based cold pool. The compression warming occurring within this subsidence region is responsible, hydrostatically, for the reduced pressure at the surface, and the column stretching implied by the subsidence favors the concentration of midlevel relative vorticity. This sequence of events was suggested by Johnson et al. (1989) as an explanation for the surface observations obtained in the 23–24 June 1985 OK PRE-STORM MCS, which clearly contained a collapsing-stratiform-region MCV.

The vertically coherent MCV observed in this study, on 29 July 2004, has several unique characteristics compared with the other MCV types. The breadth and persistence of the mesolow suggest that different dynamics are active than in the other cases. Upper-air observations from the NPN do not reveal any obvious low-level warming such as would be expected in the vicinity of

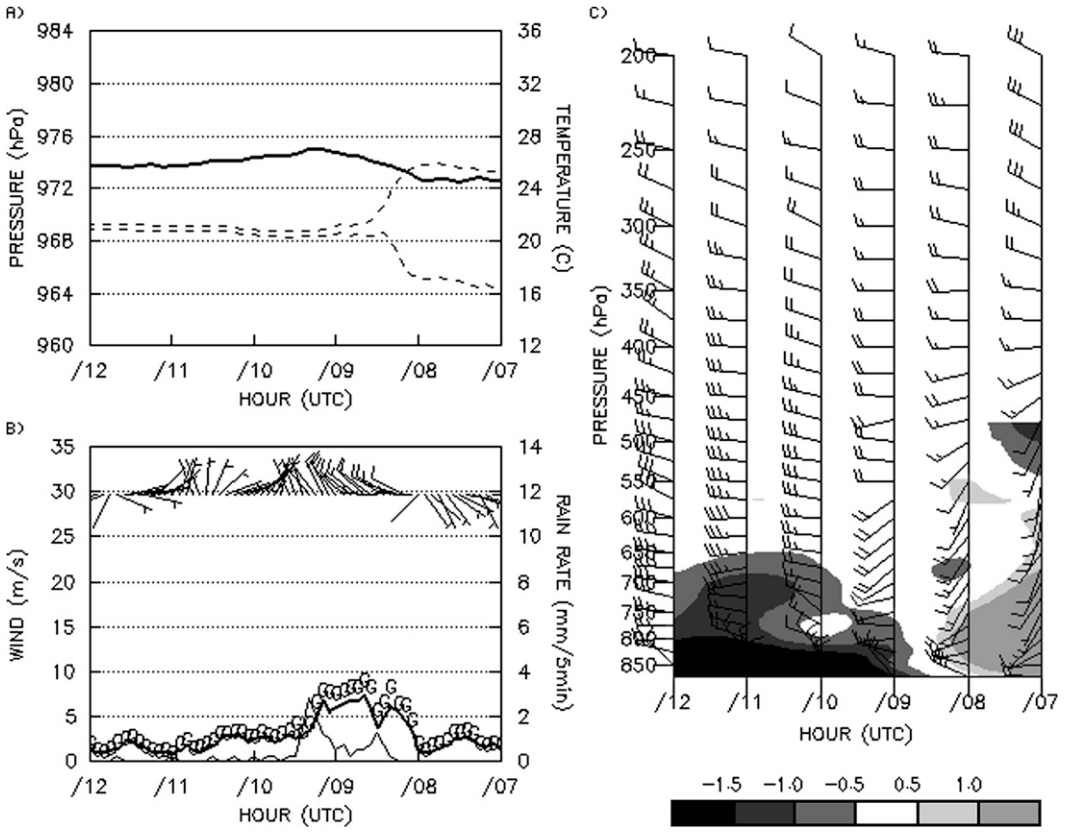

FIG. 19. As in Fig. 3, but (a),(b) for the Lahoma OM station (location marked in Fig. 18d) and (c) for the Vici NPN station (location marked in Fig. 18d), 0700–1200 UTC 30 Jul 2003.

MCVs of the first two types. However, analyses from the RUC do indicate a relatively deep warm core at the midlevels, associated with a coherent tower of high PV. The surface mesolow is apparently a hydrostatic result of the mesoscale warm core associated with the MCV. It is not immediately obvious why the warm core is so much deeper in this case than in other cases; perhaps it is related to the longevity of the precipitation shield and its

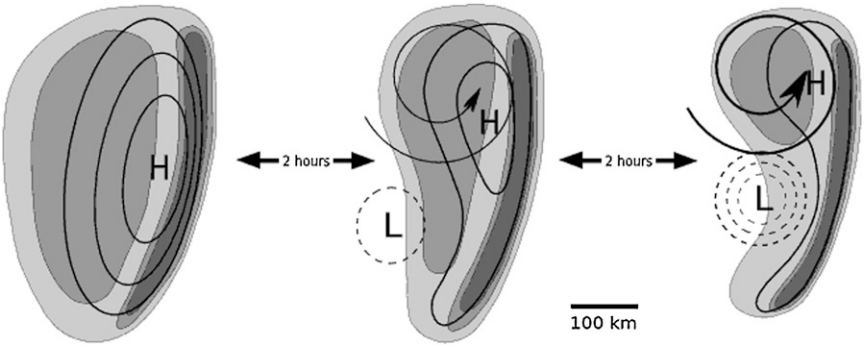

FIG. 20. Conceptual model of the typical evolution of a rear-inflow-jet MCV. Time runs from left to right, and evolution is with respect to a system moving toward the right. Shading represents composite radar reflectivity; light shading indicates 30–40 dBZ, moderate shading indicates 40–50 dBZ, and dark shading indicates >50 dBZ. Thin black lines represent isobars of surface pressure perturbation (contour interval 1 hPa; negative contours dashed). ''H'' indicates the center of the mesohigh, and ''L'' indicates the center of the mesolow. The spiral indicates the location of the developing midlevel vortex, with line thickness proportional to vortex intensity.

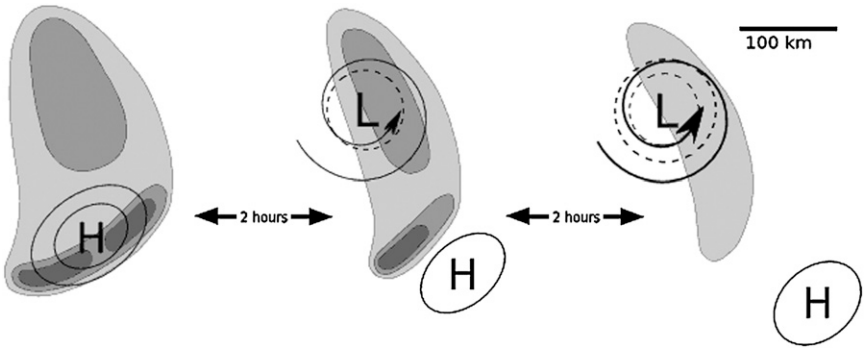

FIG. 21. As in Fig. 20, but of a collapsing-stratiform-region MCV.

associated diabatic heating. While the warm core does not appear to extend to the surface, it is also apparent that there is no well-defined surface cold pool. The weakness of the cold pool may be the defining feature allowing such a strong mesolow to form. Vertically coherent MCVs have recently been simulated by Conzemius et al. (2007) and Davis and Galarneau (2009); these authors emphasize the role of low-level convergence within a moist neutral environment in the development of a surface cyclonic circulation. We are unable to definitively determine the mechanisms responsible for the development of surface features in the 29 July 2004 MCV, because the vortex acquires a well-defined surface circulation and mesolow before moving into Oklahoma.

It is tempting to compare the vertically coherent MCV with an incipient tropical cyclone. The similarities are considerable: there is a closed surface circulation with a well-defined low pressure center, a large and deep tower of high PV extending into the mid to upper troposphere, and an extremely moist environment. The lack of any significant organization of the precipitation field, as well as the weakness of the surface wind field, may be related to the fact that the system is in its early stages of development. Soundings taken in the environment of the 29 July 2004 MCV (not shown) reveal that the atmosphere is nearly saturated, with a near-moist-adiabatic lapse rate. The lack of strong surface fluxes from an underlying warm ocean explains the failure of tropical cyclogenesis (Fritsch et al. 1994); such fluxes would likely allow the MCV to transition to a true tropical cyclone (Rogers and Fritsch 2001) given weak vertical wind shear. Past studies (e.g., Bosart and Sanders 1981) have reported tropical cyclogenesis from MCVs.

The final two types of MCVs documented in this study represent vortices that fail to develop significant mesolows. The mesolow development mechanisms active in the previous cases are not present in these MCVs for several possible reasons. The remnant-circulation MCVs (14 cases, or 31% of the total) lack significant precipitation in their vicinity; precipitation is required for the hypothesized mesolow development mechanisms active in the other MCV types. The cold-pool-dominated MCVs (three cases, or 7% of the total) contain significant precipitation, but it is likely that the deep and extensive surface cold pools mask any potential pressure perturbations due to warming aloft.

The limited extent of our study domain should be kept in mind when considering these results. More than half of the 45 MCVs documented here moved outside of Oklahoma at some point during their life cycle; during these times the surface pressure field associated with the vortices is unknown. This limitation, as well as deficiencies in the RUC model, introduces some uncertainty into the classifications. Oklahoma is only a fraction of the area frequented by MCVs in the United States, but it is likely representative. Thus, we expect our MCV classifications to hold in other portions of the central United States.

5. Conclusions

This study has described the precipitation structure and evolution of midlatitude MCVs observed over the state of Oklahoma during four years. MCV case detection was achieved with an objective algorithm developed to operate on analyses from the operational RUC model, as described by DAT. Five repeating patterns of precipitation structure and surface pressure evolution have been defined, three of which produce well-defined surface mesolows.

Several characteristics of the MCV types have potential utility for forecasters. The behavior of rear-inflow-jet MCVs implies that the detection of an MCV within a large and vigorous MCS could alert forecasters to the possibility of wake low development and the associated aviation hazard of low-level wind shear (Johnson 2001). Similarly, the evolution of collapsing-stratiform-region MCVs suggests that forecasters should be vigilant for

TABLE A1. Summary of the 45 Oklahoma MCV cases documented in this study. Longevity is defined as the number of hours the MCV is detected by the objective algorithm. Vortex radius (see DAT for definition) and relative vorticity (mean over the 600–500-hPa layer) are determined for each case at MCV maturity. MCV classification is according to the five independent MCV types identified in this paper. A plus sign after the longevity indicates that RUC data are missing at the beginning and/or end of the period of MCV detection by the objective algorithm. Radius and relative vorticity are only given for cases with valid RUC data at MCV maturity.

Start time (UTC)	Longevity (h)	Radius (km)	Relative vorticity (s^{-1})	Type
1900 15 May 2002	6	224	6.92×10^{-5}	CSR[a]
0700 17 May 2002	9+	224	1.53×10^{-4}	RIJ[b]
0900 3 Jun 2002	2+	—	—	RC[c]
0600 5 Jun 2002	1+	—	—	RIJ
0800 9 Jun 2002	28+	—	—	RC
1000 24 Aug 2002	3	185	6.63×10^{-5}	CSR
1200 27 Aug 2002	9	185	1.09×10^{-4}	RIJ
0800 21 May 2003	16	224	7.96×10^{-5}	CPD[d]
1800 23 May 2003	12	185	7.58×10^{-5}	CSR
1600 24 May 2003	24	224	1.73×10^{-4}	RIJ
0700 3 Jun 2003	8+	224	1.03×10^{-4}	RIJ
0500 12 Jun 2003	6	224	1.20×10^{-4}	RIJ
1000 20 Jun 2003	18	185	4.79×10^{-5}	RC
1100 21 Jun 2003	13	262	1.14×10^{-4}	RIJ
0000 25 Jun 2003	9+	185	2.67×10^{-5}	RC
0600 29 Jun 2003	54	262	1.68×10^{-4}	RC
0600 30 Jul 2003	12	224	9.71×10^{-5}	CPD
1200 2 Aug 2003	6	224	1.16×10^{-4}	RIJ
1200 9 Aug 2003	18	224	1.30×10^{-4}	RIJ
0900 11 May 2004	25	224	1.12×10^{-4}	RC
0500 3 Jun 2004	31	224	1.53×10^{-4}	RIJ
1200 4 Jun 2004	37	262	1.08×10^{-4}	CSR
1000 6 Jun 2004	49	262	1.34×10^{-4}	RC
1000 19 Jun 2004	15+	262	9.33×10^{-5}	RC
1800 20 Jun 2004	8+	—	—	RIJ
0000 1 Jul 2004	5	262	5.38×10^{-5}	RC
1900 1 Jul 2004	19	262	9.54×10^{-5}	RC
1800 5 Jul 2004	1	142	2.38×10^{-5}	CSR
0500 16 Jul 2004	38	185	9.25×10^{-5}	RC
0800 28 Jul 2004	10	224	6.13×10^{-5}	CPD
1300 29 Jul 2004	10	262	8.83×10^{-5}	VC[e]
2200 6 Aug 2004	1	185	3.58×10^{-5}	RC
1000 9 Aug 2004	36	224	5.54×10^{-5}	CSR
0900 11 Aug 2004	16	262	1.20×10^{-4}	RIJ
1900 15 Aug 2004	18	185	7.50×10^{-5}	RC
0300 20 Aug 2004	23	262	1.23×10^{-4}	RIJ
1200 28 Aug 2004	26	224	1.28×10^{-4}	RIJ
2100 30 Aug 2004	10	185	8.04×10^{-5}	CSR
0900 13 May 2005	6	224	1.15×10^{-4}	RIJ
1200 19 May 2005	6	224	6.96×10^{-5}	CSR
1800 6 Jun 2005	10	224	5.33×10^{-5}	RC
0500 10 Jun 2005	12	224	1.01×10^{-4}	RIJ
0600 17 Jun 2005	7	262	1.28×10^{-4}	RIJ
1100 1 Jul 2005	16	224	1.33×10^{-4}	RIJ
0800 2 Jul 2005	12	224	2.25×10^{-4}	RIJ

[a] Collapsing-stratiform-region MCV.
[b] Rear-inflow-jet MCV.
[c] Remnant-circulation MCV.
[d] Cold-pool-dominated MCV.
[e] Vertically coherent MCV.

MCV development, which may influence convective potential in the region over the next 24 h, when a broad and deep mesolow forms within the collapsing stratiform region of an MCS. Vertically coherent MCVs should be closely monitored in coastal regions during the hurricane season, as they can undergo tropical cyclogenesis over a warm ocean surface (Bosart and Sanders 1981). Extratropical cyclogenesis can also occur

from MCVs (Zhang and Harvey 1995), although this is perhaps a less significant threat because of the weak ambient temperature gradients during the warm season.

Several avenues of future research are suggested by the findings of this study. Further observations of MCVs are needed; specifically, high-resolution upper-air observations, such as can be obtained with dropsonde-equipped aircraft during field campaigns, would be helpful in diagnosing the detailed structure of MCVs. Numerical simulations of MCV evolution in a variety of environments could confirm the mesolow formation mechanisms proposed in this study. In addition, such simulations may elucidate the underlying causes for the wide variety of MCV structures and evolutions observed. Finally, the identification of distinct classes of MCVs suggests that a composite analysis of each type may be beneficial. It is anticipated that continuing research in this area will eventually lead to marked improvements in warm season forecast skill in the midlatitudes.

Acknowledgments. The Oklahoma Climatological Survey provided the Oklahoma Mesonet data used in this study. RUC analyses were obtained from NOAA's National Operational Model Archive and Distribution System. The original MCV detection algorithm was provided by David Ahijevych of NCAR. The multiquadratic analysis software was originally developed by Rebecca Adams-Selin of CSU. We thank Bob Conzemius and two anonymous reviewers for helpful comments on an earlier version of the manuscript. This research was supported by National Science Foundation Grant ATM-0500061.

APPENDIX

MCV Cases

Table A1 lists all the MCV cases included in this study. Parameters displayed for each case include the time of first detection by the objective algorithm, longevity (number of hours MCV is detected by the objective algorithm), vortex radius (see DAT for definition), relative vorticity (mean over the 600–500-hPa layer), and classification according to the five MCV types defined in this paper. The radius and relative vorticity values for each case are given at the time when the MCV reaches its maximum relative vorticity at any level between 600 and 500 hPa; this represents the mature phase of the vortex. All of these parameters are determined from the RUC analyses. The reader is referred to Table 1 for mean values of longevity, radius, and relative vorticity among each of the MCV types.

Eleven of the 45 MCVs develop before moving into our analysis domain. These vortices last between 1 and 23 h before entering Oklahoma, although most of them are at the lower end of this range. The diurnal timing of these cases' entry into Oklahoma varies between 0500 and 2200 UTC, although most of the entries occur during the early morning (0500–1400 UTC). Thus, the surface pressure features of some of the vortices are sampled at different stages of their life cycles. However, the precipitation evolution of each case can be followed with national radar imagery throughout the life cycle. For the conceptual models presented in this paper, the relevant cases have all been composited at the same points in their life cycle with respect to the mature phase.

REFERENCES

Adams-Selin, R. D., and R. H. Johnson, 2010: Mesoscale surface pressure and temperature features associated with bow echoes. *Mon. Wea. Rev.,* **138,** 212–227.

Bartels, D. L., and R. A. Maddox, 1991: Midlevel cyclonic vortices generated by mesoscale convective systems. *Mon. Wea. Rev.,* **119,** 104–118.

Benjamin, S. G., and Coauthors, 2004: An hourly assimilation-forecast cycle: The RUC. *Mon. Wea. Rev.,* **132,** 495–518.

Bernstein, B. C., and R. H. Johnson, 1994: A dual-Doppler radar study of an OK PRE-STORM heat burst event. *Mon. Wea. Rev.,* **122,** 259–273.

Bosart, L. F., and F. Sanders, 1981: The Johnstown flood of July 1977: A long-lived convective system. *J. Atmos. Sci.,* **38,** 1616–1642.

Brandes, E. A., 1990: Evolution and structure of the 6–7 May 1985 mesoscale convective system and associated vortex. *Mon. Wea. Rev.,* **118,** 109–127.

——, and C. L. Ziegler, 1993: Mesoscale downdraft influences on vertical vorticity in a mature mesoscale convective system. *Mon. Wea. Rev.,* **121,** 1337–1353.

Brown, J. M., 1979: Mesoscale unsaturated downdrafts driven by rainfall evaporation: A numerical study. *J. Atmos. Sci.,* **36,** 313–338.

Chen, S. S., and W. M. Frank, 1993: A numerical study of the genesis of extratropical convective mesovortices. Part I: Evolution and dynamics. *J. Atmos. Sci.,* **50,** 2401–2426.

Chong, M., and O. Bousquet, 1999: A mesovortex within a near-equatorial mesoscale convective system during TOGA COARE. *Mon. Wea. Rev.,* **127,** 1145–1156.

Conzemius, R. J., R. W. Moore, M. T. Montgomery, and C. A. Davis, 2007: Mesoscale convective vortex formation in a weakly sheared moist neutral environment. *J. Atmos. Sci.,* **64,** 1443–1466.

Cunning, J. B., 1986: The Oklahoma–Kansas preliminary regional experiment for STORM-Central. *Bull. Amer. Meteor. Soc.,* **67,** 1478–1486.

Davis, C. A., and S. B. Trier, 2002: Cloud-resolving simulations of mesoscale vortex intensification and its effect on a serial mesoscale convective system. *Mon. Wea. Rev.,* **130,** 2839–2858.

——, and ——, 2007: Mesoscale convective vortices observed during BAMEX. Part I: Kinematic and thermodynamic structure. *Mon. Wea. Rev.,* **135,** 2029–2049.

——, and T. J. Galarneau Jr., 2009: The vertical structure of mesoscale convective vortices. *J. Atmos. Sci.,* **66,** 686–704.

——, D. A. Ahijevych, and S. B. Trier, 2002: Detection and prediction of warm season midtropospheric vortices by the Rapid Update Cycle. *Mon. Wea. Rev.,* **130,** 24–42.

——, and Coauthors, 2004: The Bow Echo and MCV Experiment: Observations and opportunities. *Bull. Amer. Meteor. Soc.,* **85,** 1075–1093.

Fritsch, J. M., J. D. Murphy, and J. S. Kain, 1994: Warm core vortex amplification over land. *J. Atmos. Sci.,* **51,** 1780–1807.

Fujita, T. T., 1951: Microanalytical study of thunder-nose. *Geophys. Mag. Tokyo,* **22,** 78–88.

Galarneau, T. J., Jr., L. F. Bosart, C. A. Davis, and R. McTaggart-Cowan, 2009: Baroclinic transition of a long-lived mesoscale convective vortex. *Mon. Wea. Rev.,* **137,** 562–584.

Hertenstein, R. F. A., and W. H. Schubert, 1991: Potential vorticity anomalies associated with squall lines. *Mon. Wea. Rev.,* **119,** 1663–1672.

Houze, R. A., Jr., and A. K. Betts, 1981: Convection in GATE. *Rev. Geophys. Space Phys.,* **19,** 541–576.

——, S. A. Rutledge, M. I. Biggerstaff, and B. F. Smull, 1989: Interpretation of Doppler weather radar displays of midlatitude mesoscale convective systems. *Bull. Amer. Meteor. Soc.,* **70,** 608–619.

——, B. F. Smull, and P. Dodge, 1990: Mesoscale organization of springtime rainstorms in Oklahoma. *Mon. Wea. Rev.,* **118,** 613–654.

Johnson, B. C., 1983: The heat burst of 29 May 1976. *Mon. Wea. Rev.,* **111,** 1776–1792.

Johnson, R. H., 2001: Surface mesohighs and mesolows. *Bull. Amer. Meteor. Soc.,* **82,** 13–31.

——, and P. J. Hamilton, 1988: The relationship of surface pressure features to the precipitation and airflow structure of an intense midlatitude squall line. *Mon. Wea. Rev.,* **116,** 1444–1472.

——, S. Chen, and J. J. Toth, 1989: Circulations associated with a mature-to-decaying midlatitude mesoscale convective system. Part I: Surface features—Heat bursts and mesolow development. *Mon. Wea. Rev.,* **117,** 942–959.

Johnston, E. C., 1982: Mesoscale vorticity centers induced by mesoscale convective complexes. Preprints, *Ninth Conf. on Weather Analysis and Forecasting,* Seattle, WA, Amer. Meteor. Soc., 196–200.

Kirk, J. R., 2003: Comparing the dynamical development of two mesoscale convective vortices. *Mon. Wea. Rev.,* **131,** 862–890.

——, 2007: A phase-plot method for diagnosing vorticity concentration mechanisms in mesoscale convective vortices. *Mon. Wea. Rev.,* **135,** 801–820.

Knievel, J. C., and R. H. Johnson, 2002: The kinematics of a midlatitude, continental mesoscale convective system and its mesoscale vortex. *Mon. Wea. Rev.,* **130,** 1749–1770.

Loehrer, S. M., and R. H. Johnson, 1995: Surface pressure and precipitation life cycle characteristics of PRE-STORM mesoscale convective systems. *Mon. Wea. Rev.,* **123,** 600–621.

McNulty, R. P., 1991: Downbursts from innocuous clouds: An example. *Wea. Forecasting,* **6,** 148–154.

Nuss, W. A., and D. W. Titley, 1994: Use of multiquadratic interpolation for meteorological objective analysis. *Mon. Wea. Rev.,* **122,** 1611–1631.

Parker, M. D., and R. H. Johnson, 2000: Organizational modes of midlatitude mesoscale convective systems. *Mon. Wea. Rev.,* **128,** 3413–3436.

Raymond, D. J., and H. Jiang, 1990: A theory for long-lived mesoscale convective systems. *J. Atmos. Sci.,* **47,** 3067–3077.

Rogers, R. F., and J. M. Fritsch, 2001: Surface cyclogenesis from convectively driven amplification of midlevel mesoscale convective vortices. *Mon. Wea. Rev.,* **129,** 605–637.

Schumacher, R. S., and R. H. Johnson, 2008: Mesoscale processes contributing to extreme rainfall in a midlatitude warm-season flash flood. *Mon. Wea. Rev.,* **136,** 3964–3986.

——, and ——, 2009: Quasi-stationary, extreme-rain-producing convective systems associated with midlevel cyclonic circulations. *Wea. Forecasting,* **24,** 555–574.

Scott, J. D., and S. A. Rutledge, 1995: Doppler radar observations of an asymmetric mesoscale convective system and associated vortex couplet. *Mon. Wea. Rev.,* **123,** 3437–3457.

Smull, B. F., and R. A. Houze Jr., 1985: A midlatitude squall line with a trailing region of stratiform rain: Radar and satellite observations. *Mon. Wea. Rev.,* **113,** 117–133.

Stumpf, G. J., R. H. Johnson, and B. F. Smull, 1991: The wake low in a midlatitude mesoscale convective system having complex convective organization. *Mon. Wea. Rev.,* **119,** 134–158.

Trier, S. B., and C. A. Davis, 2002: Influence of balanced motions on heavy precipitation within a long-lived convectively generated vortex. *Mon. Wea. Rev.,* **130,** 877–899.

Vescio, M. D., and R. H. Johnson, 1992: The surface-wind response to transient mesoscale pressure fields associated with squall lines. *Mon. Wea. Rev.,* **120,** 1837–1850.

Zhang, D.-L., and R. Harvey, 1995: Enhancement of extratropical cyclogenesis by a mesoscale convective system. *J. Atmos. Sci.,* **52,** 1107–1127.

Zipser, E. J., 1977: Mesoscale and convective-scale downdrafts as distinct components of squall-line structure. *Mon. Wea. Rev.,* **105,** 1568–1589.